

1 **Oblique rifting triggered by slab tearing : the case of the Alboran** 2 **rifted margin in the eastern Betics**

3
4 Marine Larrey^{1,2}, Frédéric Mouthereau^{1*}, Damien Do Couto³, Emmanuel Masini⁴, Anthony
5 Jourdon⁵, Sylvain Calassou² and Véronique Miekebielle²

6 ¹Université Paul Sabatier, Géosciences Environnement Toulouse, GET UMR 5563, Toulouse, France.

7 ²TOTAL S.A., Centre Scientifique & Technique Jean Féger, Pau, France.

8 ³Sorbonne Université, CNRS-INSU, Institut des Sciences de la Terre Paris, ISTeP UMR 7193, F-75005 Paris,
9 France.

10 ⁴M&U sas, France.

11 ⁵Institute of Geophysics, Ludwig-Maximilians-Universität München, Munich, Germany.

12 *Corresponding author:* Frédéric Mouthereau (frederic.mouthereau@get.omp.eu)

13 **Abstract**

14
15 The tectonic evolution of highly oblique continental margins that result from extension above lithospheric STEP faults
16 is poorly understood. Here, we investigate the case of the Alboran margin in the eastern Betics characterized by crustal
17 thinning of 15-10 km, oblique to the direction of slab retreat. The current deformation patterns indicate that oblique
18 rifting is underway. However, it is unclear whether these conditions are those that prevailed during the formation of
19 the metamorphic domes and intramontane basins. We review the temporal and spatial evolution of Neogene
20 sedimentary basins and brittle deformation in the eastern Betics, and exploit offshore seismic reflection lines to
21 propose a crustal-scale section across the oblique margin. The history of sediment infill and rates of subsidence
22 combined with the analyses of fault slip data, confirm that brittle extension oriented from N20°E to EW occurred
23 during an interval spanning from the Serravallian-early Tortonian to the late Tortonian (14-8 Ma). This extension is
24 associated with both normal and strike-slip regimes and the evolution of the strike-slip fault zones flanking the
25 metamorphic domes. The transtensional model forms a coherent scheme linking the ductile deformation associated
26 with metamorphic domes and the formation of EW- and NW-SE/NNW-SSE-directed sedimentary basins in the brittle
27 upper crust during the Tortonian. The oblique extension, which is closely associated with STEP faulting, occurred
28 during the regional convergence between Africa and Iberia since the Miocene. Only recently, around 8 Ma, slab
29 detachment started to migrate westward, leading to tectonic inversion in the eastern Betics. Such a type of narrow
30 oblique rifted margin associated with transform-like plate boundaries is not unique but is expected to be hardly
31 preserved in the geological record due to the transient nature of retreating subduction systems.

32 **1 Introduction**

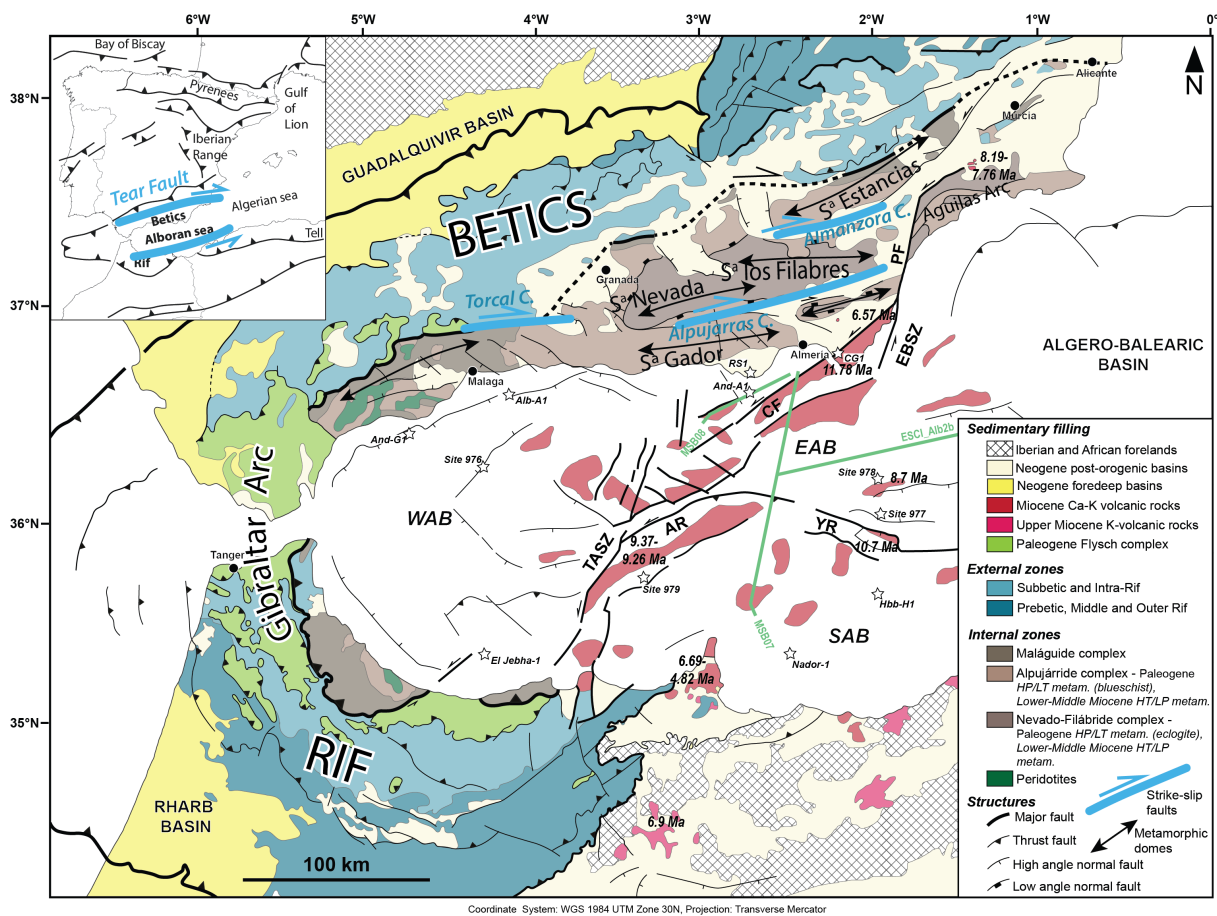
33 **1.1 Tear faulting and oblique crustal thinning in the Betics**

34 Lithospheric tear faults or subduction-transform edge propagator (STEP) faults are propagating strike-slip faults that
35 accommodate the differential motion between the retreating subduction zone and the overriding plate (Govers and
36 Wortel, 2005). Because of the relative motion between back-arc and surrounding plates, they are also propagating
37 strike-slip faults defined by a sharp contrast in crustal thickness. As noted by Govers and Wortel (2005) such oblique
38 fault boundaries do not necessarily form proper transform plate boundaries but broad zones of distributed deformation,
39 accommodating differential trench-parallel extension, strike-slip motion and rotation. In case the lithospheric tear
40 propagates within the continent-ocean transition, a narrow continental margin forms highly oblique to the direction of
41 back-arc extension. This is documented, for instance, in the Carribean, along the transcurrent Carribean-South
42 America plate boundary (Pindell and Kennan, 2009) or on the margin of the South Orckney microcontinent, along the
43 Scotia-Antarctic plate boundary (Dalziel et al., 2013). Despite the large-scale kinematic picture is relatively well
44 understood, there are only few places on Earth where continental crustal deformation associated with slab-edge
45 continental rift system can be studied both onland and offshore.

46 Here, we focus on the eastern Betic Cordillera, which constitutes a rifted margin defined by decreasing crustal
47 thickness from >35 km to 20 km onshore (Diaz et al., 2016), thinning offshore to 16-6 km in the Eastern Alboran arc
48 to back-arc region (Booth-Rea et al., 2018; Gómez de la Peña, 2020a) (**Figs 1 and 2**). This region is seen to develop
49 above a EW-trending STEP fault at the boundary between the Alboran basin and the Iberian paleomargin (Badji et
50 al., 2014; Gallais et al., 2013; Jolivet et al., 2021a; Mancilla et al., 2015a). The tectonic expression of the strike-slip
51 deformation during E-W-directed crustal extension above the lithospheric tear is however controversial. On the one
52 hand, low-angle ductile extensional detachments with a top-to-the-west sense of shear are the main features
53 accommodating deformation in the overriding plate. Yet, a-type metamorphic domes in the lower crust, elongated
54 parallel to the E-W direction (**Fig. 1**), formed during the early Miocene, are viewed to express the transtensional
55 deformation at the tip of propagating tear (Le Pourhiet et al., 2012). On the other hand, E-W-directed transfer strike-
56 slip faulting is interpreted as a late (post-middle Miocene) brittle deformation feature associated with differential E-
57 W crustal extension between the metamorphic domes in the eastern Betics (Alpujarras fault zone ; Sanz de Galdeano
58 and Vera, 1992; Sanz de Galdeano et al., 1985; Martínez-Martínez et al., 2006) and in the western Betics (Torcal fault
59 zone ; Barcos et al., 2015) unrelated to ductile deformation (**Fig. 1**). In line with the latter interpretation, the dextral
60 motion these transfer faults accommodate is assumed to be modest, reflecting a recent post-8 Ma kinematic change
61 that accompanies the stalling of westward slab rollback, the onset of tectonic inversion in the Gibraltar Arc (Do Couto
62 et al., 2014; d'Acremont et al., 2020; Jolivet et al., 2021a; Martínez-García et al., 2017), and progressive slab tearing
63 and delamination of the lithospheric mantle from the eastern to the central Betics (Martínez-Martínez et al., 2006 ;
64 Mancilla et al., 2015a ; García-Castellanos and Villaseñor, 2011; Spakman et al., 2018). Note that in a recent study
65 the dextral displacement since 9 Ma has been estimated to more than 100 km along the Torcal fault (Crespo-Blanc et
66 al., 2016).

67 The lack of structural, temporal constraints and quantification of belt-parallel motion along these faults indicates,
68 however, that we do not yet fully understand their link with the long-term evolution of slab tearing and margin

69 formation. For instance, the current deformation patterns in the Central Betics, where metamorphic domes are present,
 70 brings evidence that both strike-slip faulting and extension operate synchronously (Martínez-Martínez et al., 2006).
 71 This is shown by the west-directed GPS velocities increasing westwards indicating ongoing extension, and the west-
 72 directed displacements increasing from North to South, towards the Alboran domain, revealing right-lateral shear (**Fig.**
 73 **2**). This together with evidence for present-day 4.5 mm/yr westward displacement and rotations in the Western Betics
 74 and Rif reveal that the westward slab rollback is likely to be still ongoing (Fadil et al., 2006; Gonzalez-Castillo et al.,
 75 2015). The current transtensional deformation across the Betic Cordillera is consistent with the current stress regime
 76 defined by extension direction highly oblique (max. 20°) to the Betic structural trend (or 70° spanned by the direction
 77 of extension and normal of the rift trend).

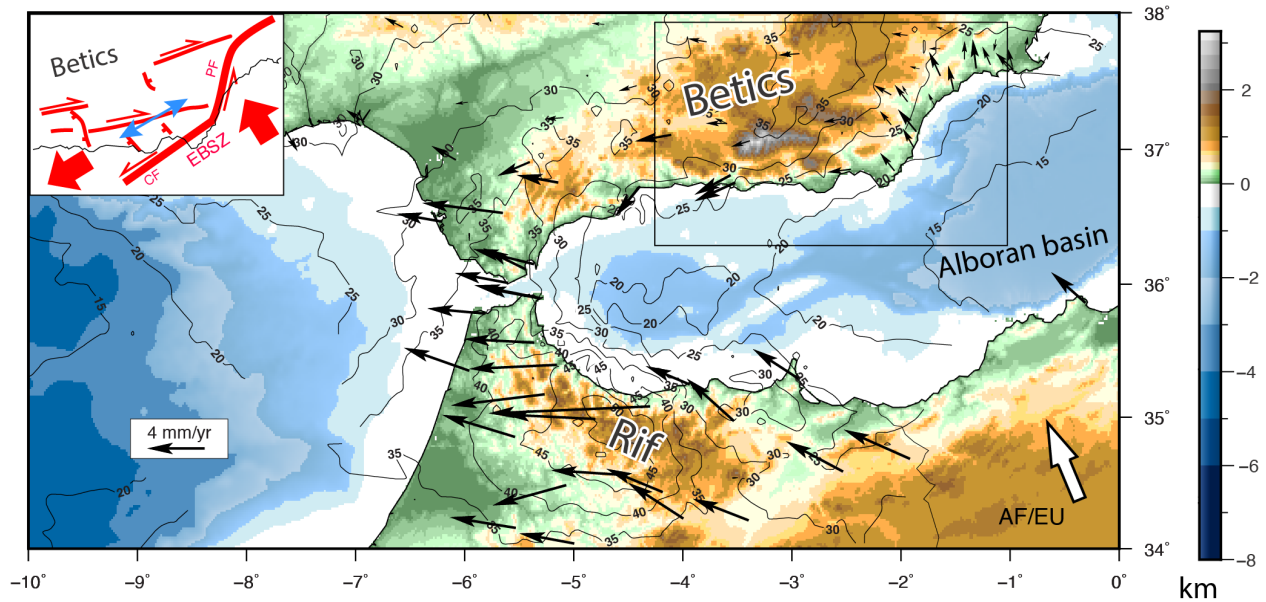


78
 79 **Figure 1** : Geological map of the Betic-Rif arc. Main tectonic units and age of volcanism as well as major structures
 80 and Neogene sedimentary basins are shown. The studied offshore seismic lines (red) is displayed as well as offshore
 81 wells and ODP sites (open star) for stratigraphic calibration in the East (EAB), South (SAB) and West Alboran basins
 82 (WAB). CF: Carboneras Fault; PF : Palomares Fault; AR: Alboran Ridge; YR: Yusuf Ridge; EBSZ : East Betic Shear
 83 Zone; TASZ: Trans-Alboran Shear Zone.
 84

85 **1.2 Highly oblique rifting triggered by slab tearing : a proof of concept in the eastern Betics**

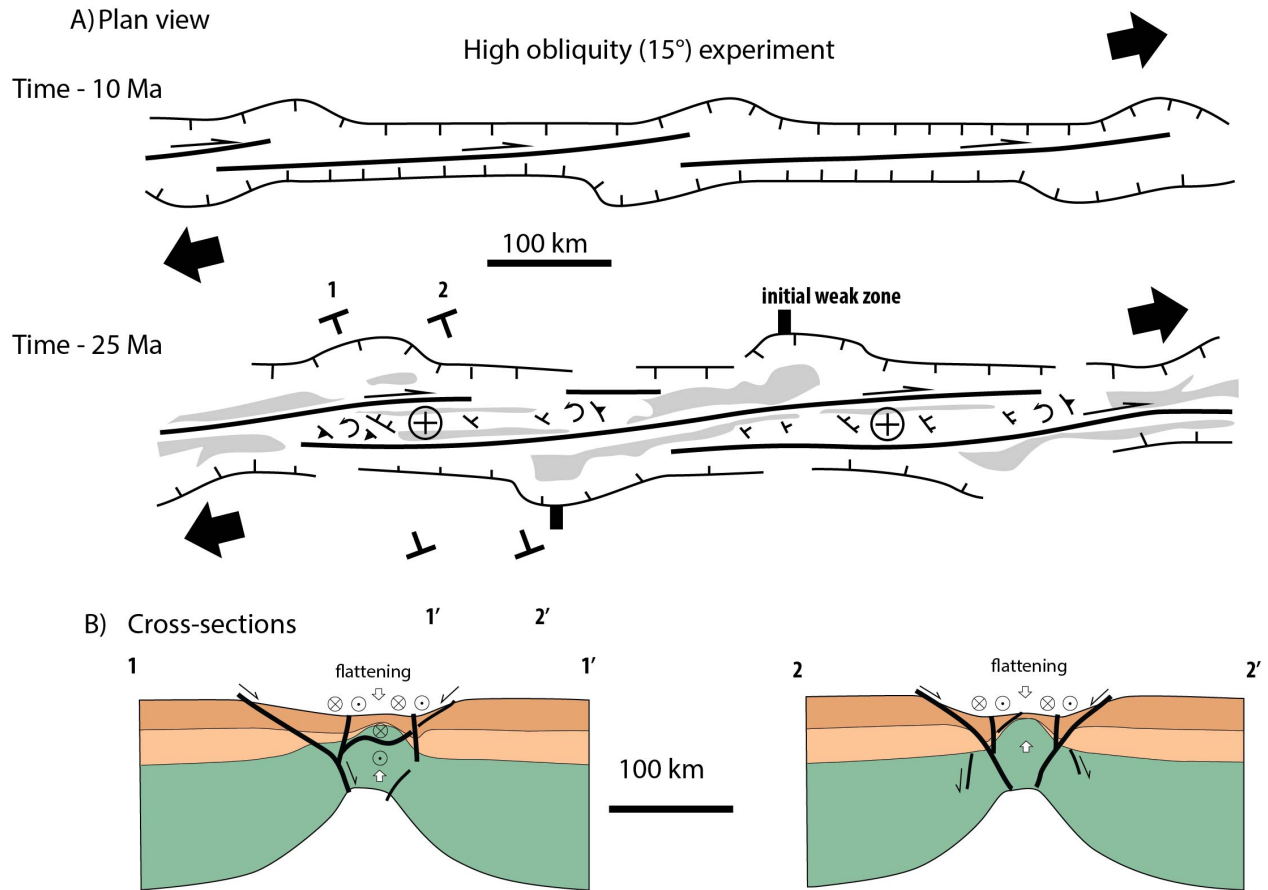
86 Right-lateral transtensional deformation in the Betics agrees with the extrusion model of the Alboran basin towards
87 the Gibraltar arc to the West (Borque et al., 2019; Palano et al., 2015) caused by indentation by the east Alboran
88 domain likely enhanced by resistance slab dragging (Spakman et al., 2018). In the East, the extrusion is accommodated
89 by left-lateral strike-slip displacement along the Eastern Betic Shear Zone (EBSZ; Borque et al., 2019), shaped by the
90 Carboneras Fault (CF) and Palomares Fault (PF), which separates the extrusion domain where extension and
91 transtension is prevailing from the Águilas Arc where N-S indentation is well documented (Ercilla et al., 2022). In
92 this region, this fault extends offshore, across the Alboran Sea, in the larger Trans-Alboran Shear Zone (De Larouzière
93 et al., 1988; Stich et al., 2006) moving at ~4 mm/yr, equivalent to the regional 5 mm/yr NW-directed convergence
94 between Africa (Nubia) and Europe (**Fig. 2**; Echeverría et al., 2013; Koulali et al., 2011; Nocquet, 2012; Palano et al.,
95 2015, 2013; Vernant et al., 2010). Here, we hypothesize that the present-day oblique extension patterns is at play since
96 the Miocene and explain the formation of the narrow Alboran rifted margin.

97 Only recently high-resolution 3D numerical models have been able to predict the deep structure of oblique rift
98 domains. These models can be used as a guide to re-evaluate the evolution of the Betics. 3D models by Jourdon et al.
99 (2021) predict that oblique extension results in narrow rifted margins, strike-slip faults and corridors coupled with
100 subsident pull-apart basins, normal faults and block rotations (**Fig. 3**). The recognition of block rotation in the Betic
101 arc (Crespo-Blanc et al., 2016; Platzman, 1992), strike-slip fault zones (**Fig. 1**) and NW-SE normal faulting, which
102 defines extension direction highly oblique to the margin (Galindo-Zaldivar et al., 2003; **Figs 1 and 2**), support this
103 view. The simulations also show that the deeper ductile crust experiences thinning (vertical flattening) and stretching
104 perpendicular to the strike of the margin in accordance with stretching lineations parallel to the metamorphic domes
105 and low-angle detachments (**Fig. 3**). Other types of 3D numerical experiments show that sediment loading of strike-
106 slip faults can result in asymmetric flexural basin with apparent normal fault throw (Neuharth et al., 2021) that can be
107 mistakenly interpreted as resulting from orthogonal extension. Asymmetric basins are indeed intriguing characteristics
108 of intramontane basins in the Betics (Rodríguez-Fernández et al., 2011; Augier et al., 2013; Do Couto et al., 2014 ;
109 Giaconia et al., 2014). Although primarily found associated with divergent plate boundaries e.g. in the Gulf of
110 California (Fossen et al., 2013; Fossen and Tikoff, 1998) highly oblique extension is also documented in active
111 transform regions along the San Andreas Fault (Teyssier and Tikoff, 1998) or the North Anatolian Fault in Marmara
112 Sea (Okay et al., 2004). A detailed analysis of highly oblique rifting deformation in the Gulf of California recognises
113 similar tectonic elements as for the Betics, such as extensional detachment systems orthogonal to the divergence and
114 upper crustal folds trending parallel to the divergence (Fossen et al., 2013).



115
 116 **Figure 2** : Present-day kinematics in the Betic-Rif arc and eastern Betic Cordillera (inset). GNSS-based displacements
 117 in the western Alboran block and north-western Africa shown in a fixed Eurasian reference frame (black arrows after
 118 Palano et al., 2015) are oblique to the AF/EU plate convergence (white arrow) inferred from plate tectonic Morvel
 119 model (Argus et al., 2011). Labelled contours depict the crustal depth given in kilometers as inferred from deep seismic
 120 profiles and receiver functions analysis (Diaz et al., 2016). In the eastern Betic (inset), W-directed stretching is taken
 121 up by EW-directed right-lateral strike-slip fault and NW-SE normal faults. Extension direction resolved from focal
 122 mechanisms (blue arrow) are after (Stich et al., 2006). CF: Carboneras Fault; PF : Palomares Fault; AR: Alboran
 123 Ridge; YR: Yusuf Ridge; EBSZ : East Betic Shear Zone; TASZ: Trans-Alboran Shear Zone.
 124

125 Several tectonic features need further discussion however. First, the relevance of strike-slip faulting in the past is
 126 debatable as only a few occurrence of crustal-scale strike-slip faults are mapped (**Fig. 1**). Second, the detail of the
 127 temporal and spatial relationships between the formation of the oblique/transform margin and STEP faulting remain
 128 elusive. We here review the temporal and spatial evolution of Neogene intramontane sedimentary basins and related
 129 brittle deformation in the eastern Betics. In addition, we exploit offshore seismic reflection lines to propose a new
 130 crustal-scale section across the oblique margin. Based on these constraints we present a tectonic scenario for the
 131 formation of the high-obliquity rifted margin controlled by STEP faulting.
 132



133

134 **Figure 3** : Sketch of highly oblique rift experiments based on the results of a 3D thermo-mechanical model (Jourdon
 135 et al., 2021). Results are depicted in plan view (A) and cross-sections (B) for two steps (after 10 Myrs and 24 Myrs)
 136 for the case where extension is set with an angle of 15° with respect to the rift axis. Grey regions in (A) are basins
 137 adjacent to uplifted domains (cross-circle symbol) associated with right-lateral strike-slip faults. Cross-sections (B)
 138 depict the abrupt crustal thinning that occur perpendicular. Crustal thinning is most visible for the lower crust and
 139 produces the formation of an abrupt necking domain controlled by rift-parallel normal faults dipping towards the
 140 center of the rift and right-lateral strike-slip faults.

141

142 2. Geodynamics and STEP faulting in the Betics

143 The onset of N-directed movement of Africa, by the Late Cretaceous-Paleogene, led to far-field, Laramide-like
 144 contraction from Morocco throughout Western Europe (Mouthereau et al., 2021). South of Iberia, in the Betic-Rif
 145 domain, the closure of hyper-extended rift systems and oceanic basins of the Atlantic-Alpine Tethys resulted in the
 146 development of a proto-Betic accretionary prism, likely largely submerged (Angrand and Mouthereau, 2021; Daudet
 147 et al., 2020; Vergés and Fernández, 2012). By about 50 Ma, the acceleration of plate convergence led to the shortening
 148 of continental rift and oceanic basins and topographic uplift all over Iberia (Daudet et al., 2020; Mouthereau et al.,
 149 2021, 2014; Rat et al., 2019; Vacherat et al., 2016; Waldner et al., 2021) associated with the onset of continental rifting
 150 along the Western European Rift (e.g. Mouthereau et al., 2021). 35 Ma ago, as Africa convergence slowed down, the
 151 western Mediterranean sea opened accompanied by retreating slabs (Dewey, 1988; Dewey et al., 1989; Faccenna et
 152 al., 2014; Jolivet and Faccenna, 2000; Rosenbaum et al., 2002). Subduction occurred mainly before 30 Ma as argued
 153 by age constraints on high-pressure mineral assemblages (Augier et al., 2005a; Bessièrè et al., 2021; Booth-Rea et al.,

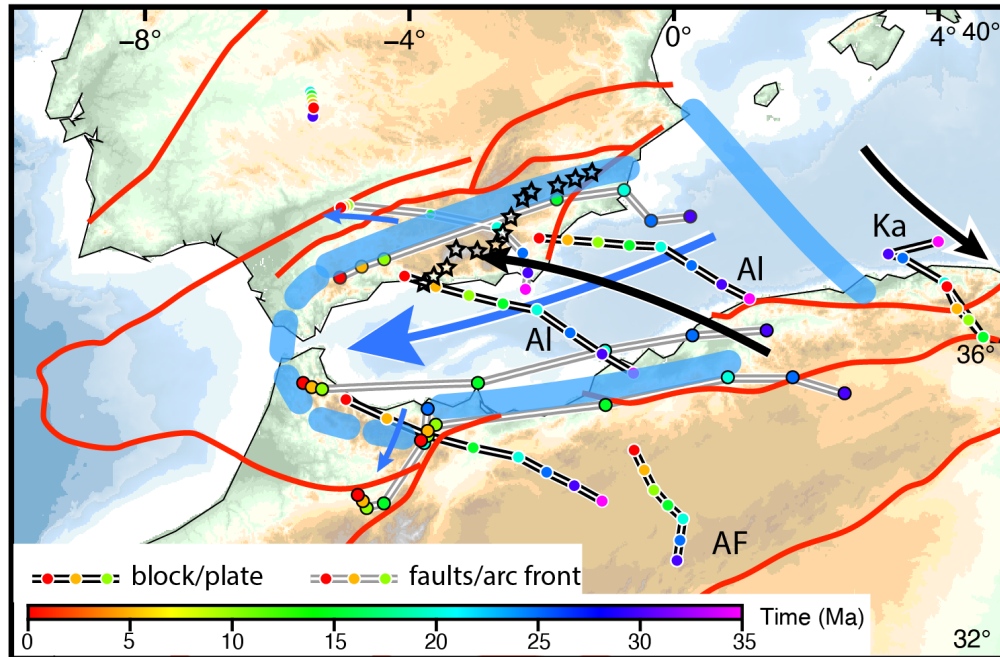
154 2015; Gomez-Pugnaire and Fernandez-Soler, 1987; Platt and Vissers, 1989; Platt and Whitehouse, 1999) and has been
155 suggested to last until the mid-Miocene in the eastern Betics e.g. (Platt et al., 2013). The timing of formation of the
156 Alboran basin is constrained to 23 to 16 Ma by the oldest deposits found on Alboran basement and by the timing of
157 high-temperature metamorphic overprint and rapid cooling to shallow crustal temperature (Bessière et al., 2021;
158 Daudet et al., 2020; Janowski et al., 2017; Johnson et al., 1997; Platt et al., 2005; Sosson et al., 1998; Vázquez et al.,
159 2011; Zeck et al., 1992). The eastern Alboran basin formed later, mostly by late Miocene arc magmatism (Booth-Rea
160 et al., 2007; 2018; Gómez de la Peña et al., 2020a).

161 All kinematic reconstructions agree that extension results from the westward migration of the arc front and retreat of
162 the Alboran slab, well imaged below the Gibraltar arc as a steeply-dipping high-velocity anomaly (Bezada et al., 2013;
163 Heit et al., 2017; Mancilla et al., 2018, 2015a, 2015b; Palomeras et al., 2014; Spakman and Wortel, 2004; Villaseñor
164 et al., 2015). These reconstructions, however, differ according to the paleo-position of Alboran terrane, and hence to
165 the amount and vergence of subduction (Angrand and Mouthereau, 2021; van Hinsbergen et al., 2014; Lonergan and
166 White, 1997; Romagny et al., 2020; Rosenbaum et al., 2002; Vergés and Fernández, 2012). Seismic tomography
167 reveals that slab detachment and tearing occur along the conjugate Alboran margins of the southern Betics and
168 northern Africa (Govers and Wortel, 2005; Heit et al., 2017; Mancilla et al., 2015a; Meighan et al., 2013; Spakman
169 and Wortel, 2004).

170 In **Fig. 4** we refer to the reconstruction of Angrand and Mouthereau (2021) that has the advantage of reconciling
171 previous western Mediterranean models (Romagny et al., 2020; Vergés & Fernández, 2012) with recent
172 thermochronological analyses in western Betics (Daudet et al., 2020) and other geological data (see compilation in
173 Mouthereau et al., 2021). This model considers that the Alboran domain has been rifted from Iberia during the Jurassic.
174 It is in agreement with detrital and igneous zircon U-Pb ages that suggest Alboran was attached to Iberia in the late
175 Paleozoic (Jabaloy-Sánchez et al., 2021). It also accounts for the existence of an upper Cretaceous-Paleogene foreland
176 basin that formed adjacent to a proto-Betic orogen and in continuity eastwards with the Balearic Promontory. In that
177 respect, it contrasts with other models placing the Alboran domain to the south of the Balearic Promontory (Moragues
178 et al., 2021; van Hinsbergen et al., 2014).

179 In this reconstruction about 400 km of slab retreat is estimated since about 35 Ma (gray path, blue arrows in **Fig. 4**).
180 It is worth noting that for Romagny et al. (2020) a similar amount (i.e. 400 km) is accommodated by back-arc extension
181 of the Alboran crust, implying the same magnitude of displacement along the STEP fault in the Betics. In the
182 reconstruction of Angrand and Mouthereau (2021), however, crustal thinning in Alboran basin is linked to
183 delamination retreat of the Alboran lithospheric mantle towards the west. Because of the decoupling between crust
184 and mantle, the length of the delaminated slab resolved at depth in seismic tomography, should not be simply translated
185 into the amount of E-W crustal extension in the Alboran domain. This further implies that the displacement across the
186 STEP fault must be also less than 400 km. Daudet et al. (2020) suggested that an extension of 110 km estimated from
187 the restoration of low-angle detachment systems in the central and eastern Betics (Martínez-Martínez et al., 2002) is
188 likely to be a more accurate crustal estimate of the movement Alboran domain rather than the total slab length.

189



190

191 **Figure 4:** Kinematics of African plate (AF), Alboran (Al) and Kabyliides (Ka) blocks with respect to fixed European
 192 plate since 35 Ma reconstructed after Angrand and Mouthereau (2021). Thick blue lines depicts the approximate
 193 position of lithospheric tear faults (between Al and Europe and Africa) and transfer faults (between Al and Ka). Tear
 194 faults located in Betics and Rif are after Jolivet et al. (2021b). Black stars depicts the positioned of tear fault in the
 195 Betics as defined by Mancilla et al. (2015a). Black arrows indicate the movement of Al and Ka with respect to Europe
 196 along black motion paths presented from 35 Ma to present. Grey motion paths refer to the motion of specific structures
 197 relative to Europe, including the motion of the arc front (thick blue dashed line) and faults in red. Dark blue arrow
 198 depicts the movement of the arc front due to retreating delamination towards the west.
 199

200 3. Miocene extension in the eastern Betics

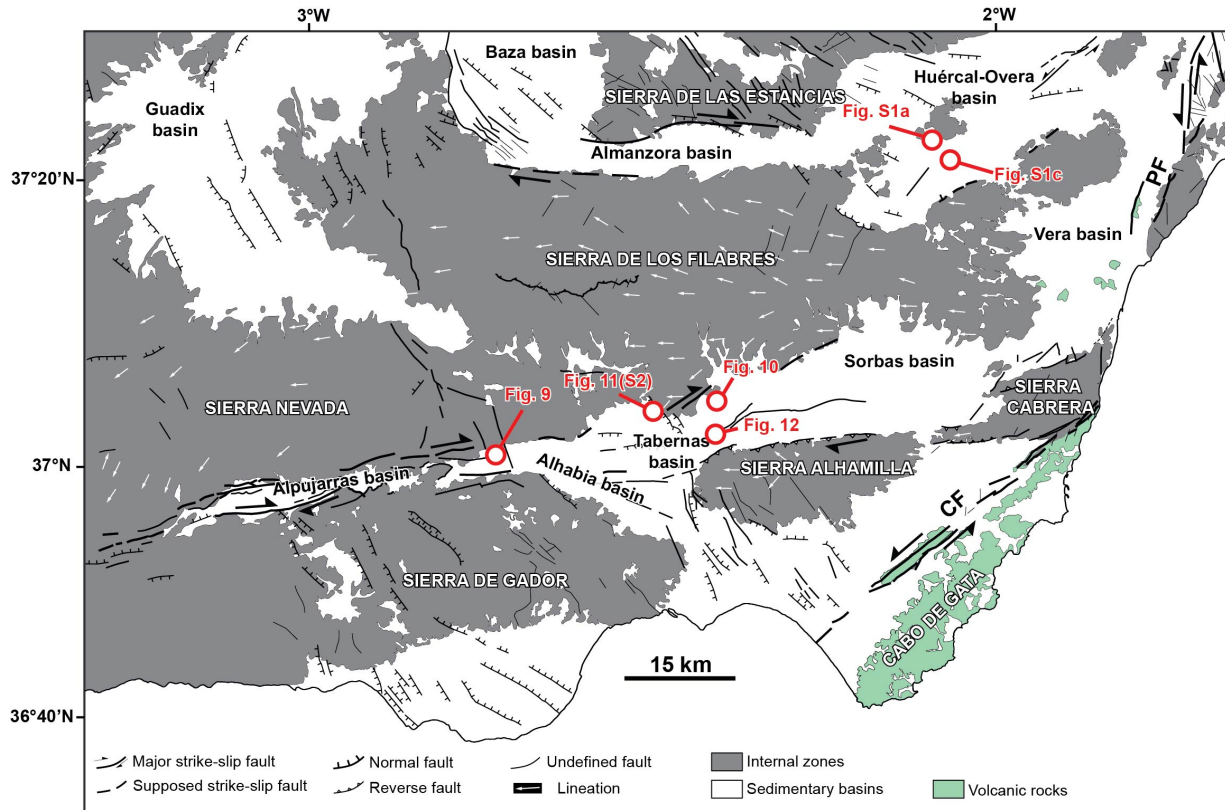
201 3.1 Relationships between domes and basins : from transtension and pure extension to late tectonic inversion

202 The most prominent extensional features in the eastern Betics are : 1) E-W elongated ranges that formed metamorphic
 203 domes with foliations bearing prominent E-W stretching lineations, for instance, in the Nevado-Filabrides
 204 Complex (**Fig. 5**; e.g. Sierra de los Filabres, Sierra Nevada, and the Sierra de las Estancias) and Serravallian-Tortonian
 205 sedimentary basins (Tabernas-Sorbas, Alpujarras, Almanzora and Huércal-Overa basins); 2) NNW-SSE/NW-SE
 206 normal fault systems and basins oblique to the domes such as the NW-SE trending Guadix-Baza and Alhabia basins
 207 (Galindo-Zaldivar et al., 2003; Martínez-Martínez and Azañón, 1997) (**Fig. 5**). They are described as asymmetric half
 208 grabens (Do Couto et al., 2014; Martínez-Martos et al., 2017; Pedrera et al., 2010, 2009) formed during the Upper
 209 Serravallian-Early Tortonian (Augier et al., 2005b; Augier et al., 2013; Meijninger and Vissers, 2006). Several of
 210 these NW-SE faults are active and cut across the metamorphic domes and the sedimentary basins (Augier et al., 2005a;
 211 Booth-Rea et al., 2004a; Giaconia et al., 2012; Montenat and Ott d'Estevou, 1999).

212 In addition to these structures, there are E-W right-lateral strike-slip fault zones and parallel depressions, like the
 213 Alpujarras fault zone between the Sierra de Gádor and the Sierra Nevada, and the Almanzora fault zone between the
 214 Sierra de los Filabres and Sierra de las Estancias (**Fig. 5**). The left-lateral Carboneras and Palomares fault system

215 (Reicherter and Hübscher, 2006; Scotney et al., 2000) marks the tectonic limit with the Cabo de Gata volcanic province
 216 (Fig. 5).

217 The domes are extension-related features interpreted either as 1) EW-metamorphic domes resulting from the
 218 exhumation in the footwall of a regional W-directed extensional low-angle detachments, later folded during post-
 219 Tortonian N-S contraction (Martínez-Martínez and Azañón, 1997; Martínez-Martínez et al., 2002, 2004) or 2)
 220 Miocene metamorphic domes formed by constrictional ductile strain regime accompanying W-directed stretching of
 221 the Alboran domain and trench retreat, with limited overprint by the Tortonian contraction ca. 8 Ma (Augier et al.,
 222 2013; Augier et al., 2005; Augier et al., 2005b; Galindo-Zaldivar et al., 2015; Jolivet et al., 2021b; Martínez-Martínez
 223 et al., 2002). Low-temperature constraints from the Nevado-Filabride and Alpujarride complexes confirm the west-
 224 directed exhumation of the basement that occurred progressively from the Sierra de los Filabres at ~13-11 Ma
 225 (Serravallian) in the East to the Sierra Nevada at 8-6 Ma (Late Tortonian-Messinian) in the West (Clark and Dempster,
 226 2009; Janowski et al., 2017; Johnson et al., 1997; Platt et al., 2005; Reinhardt et al., 2007; Vázquez et al., 2011).
 227



228
 229 **Figure 5** : Tectonic map of the eastern Betics showing the main structural elements in black after Augier et al. (2005)
 230 and Do Couto (2014). CF: Carboneras Fault; PF : Palomares Fault.
 231

232 Tectonic models for the formation of Neogene intramontane sedimentary basins vary depending on the prevailing
 233 tectonic regime. EW-directed basins have been early described as pull-apart basins (e.g Alpujarran fault zone; Sanz
 234 de Galdeano et al., 1985). Structural analyses then led to re-interpret these structures as transfer zones resulting from
 235 differential extension between exhuming core-complexes (and detachment systems) since the Serravallian (13-11 Ma)

236 later refolded during Tortonian (9-8 Ma) compression in the Eastern Betics while extension is still active in the Central
237 Betics (Martínez-Martínez et al., 2006). Other authors proposed that NE-SW extension lasted until 7.5-7 Ma in the
238 Eastern Betics (Booth-Rea et al., 2004b; Giaconia et al., 2014).

239 In support to the compressional stress regime in the Eastern Betics, Martínez-Martos et al. (2017) interpreted the E-
240 W depressions are related to the tectonic reactivation of crustal weakness zone as dextral strike-slip faults in a
241 counterclockwise rotation, accommodating part of the the N-S shortening. There are evidence that at the end of the
242 Tortonian a regional uplift occurred, rising the remnants of late Tortonian marine platform, 7.2 Ma in age, to 1600 m
243 above sea level in the Sierra de Gádor (Braga et al., 2003; Janowski et al., 2017), coincidentally with the onset of
244 contraction in the Sierra Alhamilla and Sierra de los Filabres (e.g. Do Couto et al., 2014), in the Alboran domain (e.g.
245 Martínez-García et al., 2017) and on the margins of the eastern Betic (Giaconia et al., 2013 ; 2015). In addition to
246 shortening, this recent uplift may reflect deep mantle mechanisms like slab tearing or delamination (e.g. Duggen et
247 al., 2003; García-Castellanos and Villaseñor, 2011; Mancilla et al., 2015a).

248 Based on the prevalence in some EW-trending basins, like the Huércal-Overa basin, of EW-trending normal faults,
249 these basins have alternatively been interpreted as resulting from late exhumation stage of the domes, possibly as soon
250 as the Serravallian, but mostly after the early Tortonian (syn-sedimentary faulting) (Augier et al., 2013; Augier et al.,
251 2005b; Meijninger and Vissers, 2006). The NW-SE/NNW-SSE sedimentary basins (Guadix, Baza, Alhabia; **Fig. 5**),
252 in contrast, are extensional basins formed parallel to the direction of the regional compression (Sanz de Galdeano and
253 Vera, 1992; Larouzière et al., 1988). E-W strike-slip fault zones, aligned in the direction of the domes, and NW-SE
254 normal faulting patterns are both key features consistent with predictions from models of oblique extension at
255 transform margin (**Fig. 3**). Yet, based on existing structural and tectonic syntheses a clear temporal relationships
256 between E-W ductile stretching in the domes and transcurrent deformation is not established (**Fig. 5**).

257

258 **3.2 Is the Tortonian rift-related subsidence consistent with oblique extension ?**

259 The stratigraphic architecture and depositional evolution of Tortonian intramontane basins provides first-order
260 informations on the distribution of crustal thinning. Among the oldest sediments deposited unconformably on the
261 Paleozoic-Triassic basement are the red alluvial conglomerates and deltaic series dated from the Serravallian to the
262 Lower Tortonian (**Fig. 6a**). They are thicker and well exposed on the flanks of the Almanzora basin and on the northern
263 Huércal-Overa basin (HOB), compared to the Alpujarras Corridor (AC) and Tabernas basin (TB) (**Figs. 6 and 7a**;
264 Augier et al., 2013; Pedrera et al., 2010, 2007; Poisson et al., 1996). In the east of the Sorbas basin, it should be noted
265 that Langhian-Serravalian deposits and perhaps sediments as old as Burdigalian have been locally reported (Giaconia
266 et al., 2014).

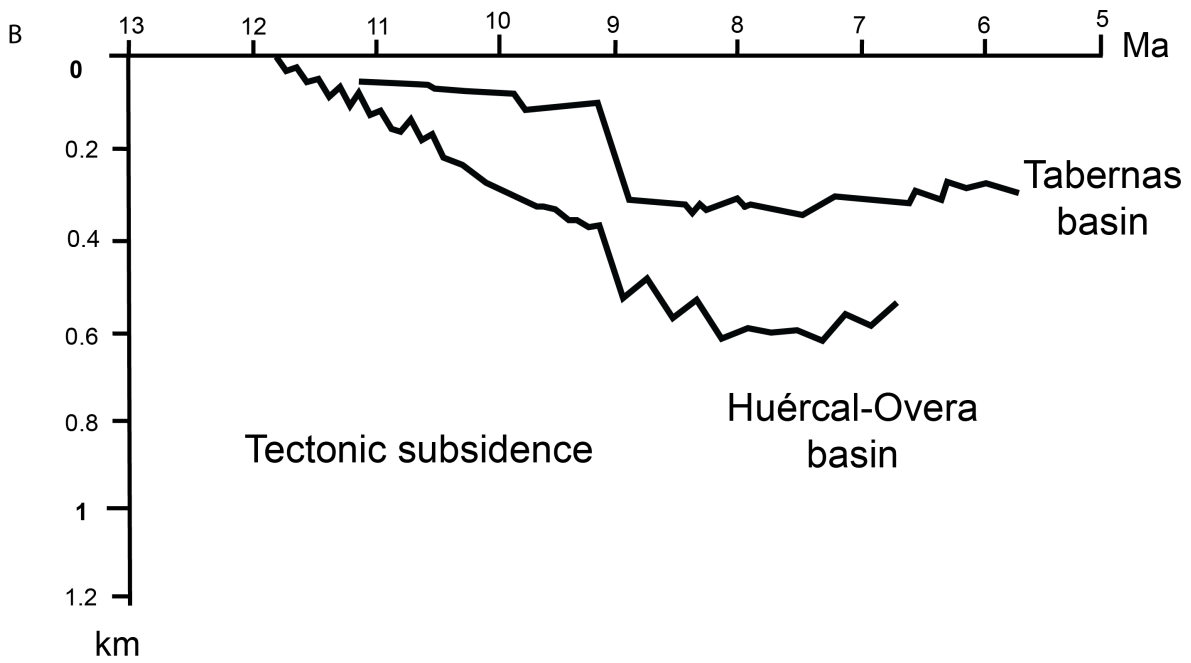
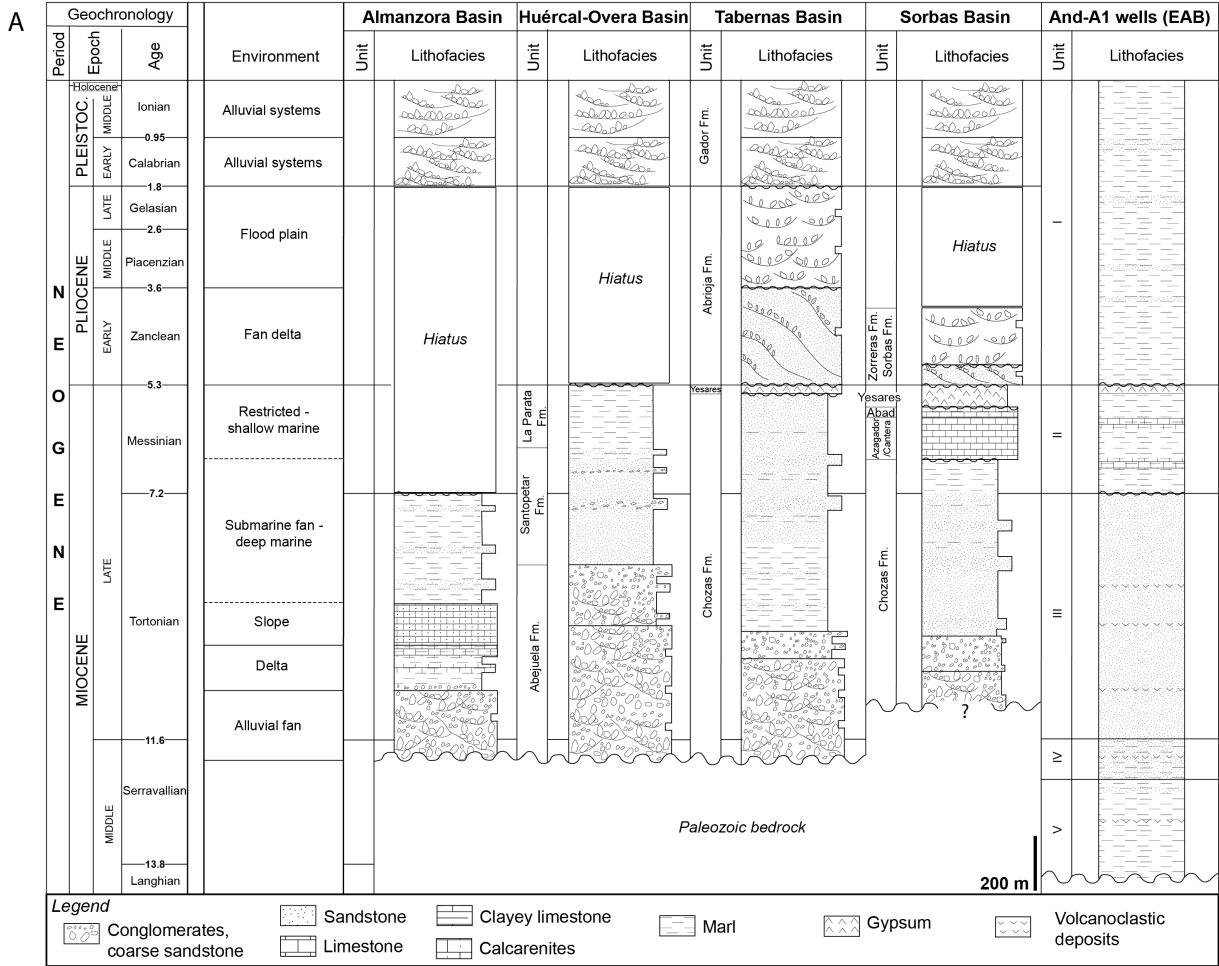
267 Paleogeographic reconstructions indicate that these Serravallian to Lower Tortonian sediments were deposited on a
268 large emerged domain, stretching from Huerca-Overa to Granada, in the West and in Tabernas, to the South (Braga
269 et al., 2003). Sourced from the Nevado-Filabride metamorphic complex (Hodgson and Haughton, 2004; Kleverlaan,
270 1989; Meijninger and Vissers, 2006; Pedrera et al., 2010, 2007; Pickering et al., 2001; Weijermars et al., 1985) these
271 deposits mark the onset of surface exhumation of the Sierra de Las Estancias and Sierra de Los Filabres.

272 During this initial stage, HOB is the most subsident basin (**Figs. 6b, 7a and 7b**), accumulating sediments at rates of
273 400 m/Ma while rates are 140-180 m/Ma in the Tabernas basin (**Fig. 6b**) (Augier, 2005). Higher subsidence in the
274 HOB, which also started earlier than in other basins, suggests extension occurred originally to the North associated
275 with the exhumation of the Sierra de Las Estancias. Basal continental conglomerates are overlain by grey coarse-
276 grained Tortonian sandstones found occasionally, e.g. in the Almanzora basin, intercalated with marine marls (**Figure**
277 **6a**). They are topped by mid-Tortonian bioclastic calcarenite and coral reefs (Braga et al., 2003; Martin et al., 1989;
278 Pedrera et al., 2007).

279 During the same interval, TB recorded the deposition of 300 to 400 m of coarse to medium-grained deltaic marine
280 clastics overlying unconformably the lowermost red series (**Fig. 6a**). These sediments pass upwards, e.g. in TB, to
281 deeper marine 1200 m-thick turbiditic and marls series intercalated with regional-scale megabeds, revealing the onset
282 of rapid tectonic subsidence (Haughton, 1994; Kleverlaan, 1989, 1987; Pickering et al., 2001; Weijermars et al., 1985).
283 Details of depositional architecture of the Tortonian suggest that part of this subsidence evolution was controlled by
284 E-W dextral strike-slip faults (Haughton, 2000 ; Baudouy et al., 2021) under transtensional strain.

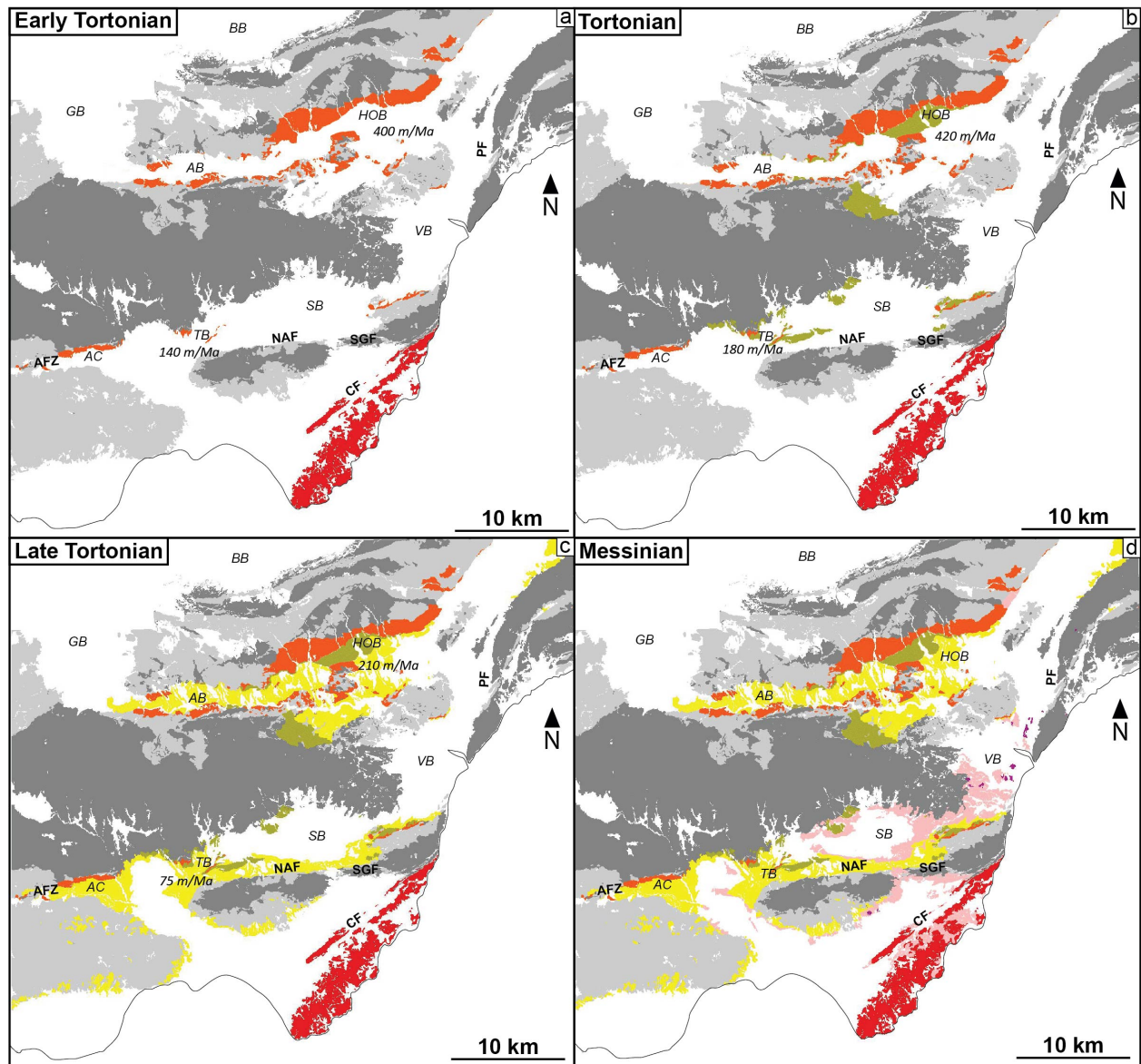
285 The transition from continental to deep marine sedimentary environments (water depth of 400-600 m according to
286 Poisson et al., 1999) witnesses the rapid rift-related tectonic subsidence achieved during the upper Tortonian times
287 (~9 Ma; **Figs. 6 and 7c**) (Augier et al., 2005b; Montenat and Ott d'Estevou, 1992; Weijermars et al., 1985). At around
288 8 Ma, accumulation rates drop by a factor of two to 200 m/Ma in HOB and 70 m/Ma in TB, revealing a marked
289 reduction in subsidence. Subsidence then became negative as basement uplifted from around 7 Ma (**Figs. 6b and 7d**)
290 in both TB and HOB.

291
292



294 **Figure 6** : Stratigraphic evolution and lithologies of intramontane basins in the eastern Betics and offshore A1 well.
295 (a) Neogene stratigraphy and basin-fill correlation in the Almanzora and Huercal-Overa basins (Mora, 1993), Tabernas
296 basin (Hodgson and Haughton, 2004; Kleverlaan, 1989; Pickering et al., 2001) and Sorbas basin (Fortuin and
297 Krijgsman, 2003; Martín and Braga, 1994; Riding et al., 1998). Middle Miocene sedimentary environments in the
298 Alboran Sea are after (Comas et al., 1992). (b) Neogene tectonic subsidence evolution for Tabernas basin and Huércal-
299 Overa basin are from Augier (2004). The curves are obtained from backstripping techniques incorporating eustatic
300 and paleobathymetric corrections. Question mark beneath the Sorbas basin lithofacies column indicates the potential
301 for uncertainty/variability across the basin (see text).
302

303 The geometry of the Almanzora (Pedrera et al., 2009), Sorbas (e.g. Do Couto et al., 2014) and Huércal-Overa basin
304 basins (Pedrera et al., 2010) inferred from gravity measurements indicate that these basins are asymmetrical and
305 deepening southwards. This sediment infill pattern recalls the formation of asymmetrical basins predicted by
306 numerical models of flexural strike-slip basins (Neuharth et al., 2021). According to this model, the asymmetry
307 observed should reflect the development of strike-slip basins loaded by sediments originated from the North. In
308 addition, a larger subsidence in HOB is an indication of abrupt crustal thinning to the south of Sierra de las Estancias
309 where the crustal thickness is the largest (**Fig. 2**). Therefore, at least the Serravallian-Tortonian infill patterns agree
310 with oblique extension.
311



312 **Figure 7:** Distribution of (a) lower Tortonian, (b) Tortonian, (c) upper Tortonian and (d) Messinian deposits based on
 313 geological mapping of the different basins. CF: Carboneras Fault; PF : Palomares Fault; SGF: South Gafarillo fault;
 314 NAF: North Alhamilla fault; AFZ: Alpujarras fault zone; BB: Baza basin; GB: Guadix basin; AB: Almanzora basin;
 315 HOB: Huercal-Overa basin; VB: Vera basin; SB: Sorbas basin; TB: Tabernas basin; AC: Alpujarras Corridor.
 316
 317

318 4. Brittle faulting : pure extension versus transtensional deformation in Neogene basins

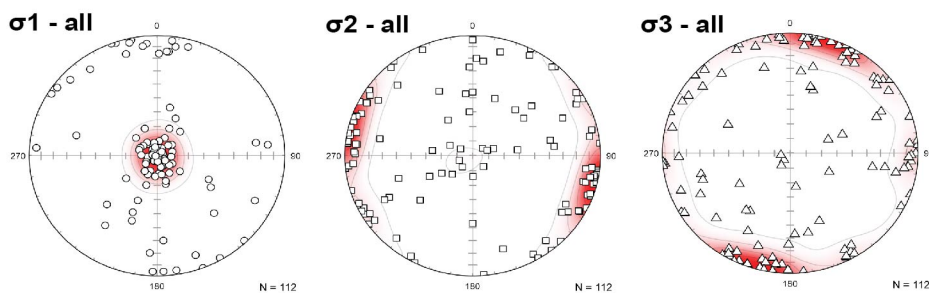
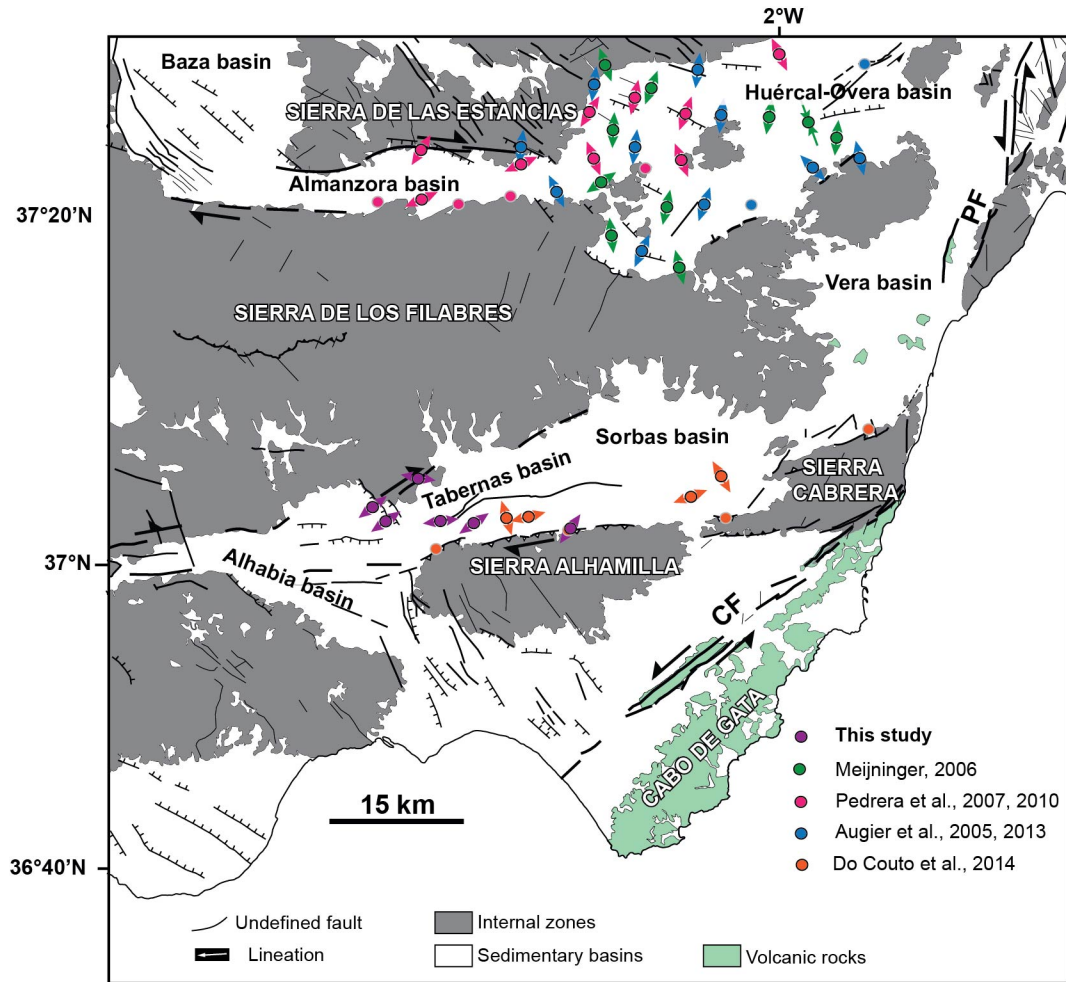
319 4.1. Tectonic regime in the eastern Betics

320 **Figure 8** presents a compilation of 112 fault slip data inversion previously analysed in the eastern Betics combined
 321 with new measurements conducted in the Alpujarras Corridor and in the Tabernas basin (**Table S1**). Most faults are
 322 syn-Tortonian or cut through the Tortonian. This compilation emphasizes a regional trend of σ_3 stress axes oriented

323 NNE-SSW (N20°E) with subordinate σ_3 oriented E-W. In details, this well-defined regional horizontal extension
324 reflects a combination of pure normal faulting regime (σ_2 horizontal and oriented NW-SE/WNW-ESE, 73% of stress
325 tensors) and strike-slip faulting regime (σ_2 vertical to steeply-dipping and σ_1 horizontal an striking NNW-SSE, 27%
326 of stress tensors). N-S to NW-SE compression is also reported in the HOB associated with incipient synform and
327 depocenter which is dated to the lower Tortonian coeval with the prominent EW/WSW-ENE extension (e.g. Pedrera
328 et al., 2010).

329 We describe below, based on a selection of outcrops in the vicinity of the contact between Tortonian basins and major
330 metamorphic domes, the expression of EW and NW-SE extensional faulting in the field. We then discuss how they
331 are linked to the regional stress regimes.

332



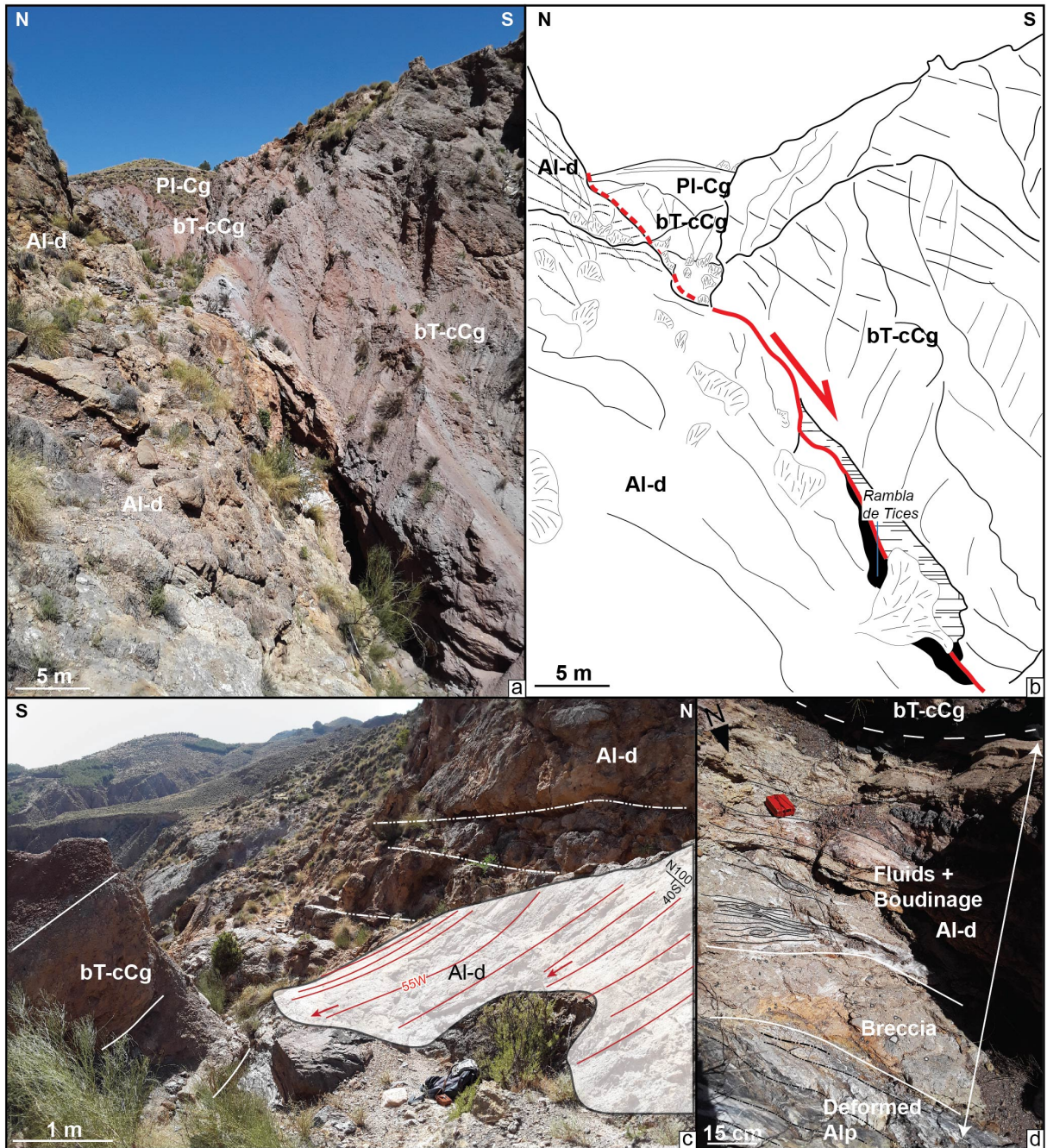
333
334
335
336
337
338
339
340

Figure 8: Synthesis of stress regimes resolved from fault slip data inversion in Tortonian basins. Color-coded circles with arrows depict tectonic sites where extension (given as arrows) is horizontal (pure extensional or strike-slip stress regimes). Sites where reverse tectonic regimes prevail are shown as circles highlighted in grey. Below, stereoplots of paleostresses σ_1 , σ_2 and σ_3 show a compilation of all brittle tectonic regimes extracted from Table S1. Collectively they define a prominent extension oriented NNE-SSW with a subordinate E-W-striking extension. CF: Carboneras Fault; PF : Palomares Fault.

341 4.2 EW-trending faults: evidence for pre-Tortonian oblique extension ?

342 In Tortonian intramontane basins, one of the main set of faults is represented by E-W-directed faults, including ENE-
343 WSW to ESE-WNW sets. North of the Alpujarras Corridor (AC), 3 km to the NE of Canjáyar, the contact between
344 the basal Tortonian conglomerates and the series of Alpujarride complex is exposed in the Rambla de Tices. It is

345 shaped by a 2-meter thick fault zone (**Figs. 9a,b**) striking N100°E, which has a normal sense of slip with a right-lateral
346 strike-slip component (**Fig. 9c**). It consists of cataclastic breccias and sheared blocks (boudins) of the host rocks (**Fig.**
347 **9d**). This major fault is found along the 65 km-long Alpujarras fault zone described by Martínez-Martínez (2006) as
348 a major strike-slip dextral transfer zone south of the Sierra Nevada that accommodates both WSW-extension and dextral
349 movement. It is mechanically consistent with NE-SW/ENE-WSW extension under a strike-slip regime as resolved
350 nearby along the same faults system (Martínez-Martínez, 2006). **Fig. 9** indicates the fault is parallel to the basal
351 Tortonian series but cuts across the Alpujarride complex. In the HOB, on the southern flank of the Sierra Limaria
352 (**Fig. 8**), the unconformity between the lower Tortonian red conglomerates and the Alpujarride units (Rambla de
353 Cordoba, 2km NW Arboleas, **Figs. S1a, b**) is found reactivated as a normal fault with a dextral shear component.
354 To the North of TB, a large morphological surface presents a rare exposure of the micaschist basement of the Nevado-
355 Filabrides complex allowing the study of deformation on the southern flank of the Sierra de los Filabres (**Fig. 10**). The
356 deformed NF series shapes a kilometric-size antiform with axial planar surface dipping towards the North. The steeply-
357 dipping cleavages directed NE-SW on its southern flank are deformed by numerous dextral shear zones with lengths
358 ranging from 100 m to less than 5 m (**Fig. 10b, c**). In addition to isoclinal folds parallel to the main foliation that are
359 clearly associated to an early stage of ductile EW-stretching, we recognize close to the strike-slip shear zones, steeply-
360 dipping metric-size open to tight folds inclined to the NE (**Fig. 10d**). To the south, Tortonian conglomerates are
361 overlying unconformably the folded NF foliation. This stratigraphic relationships and the average low dip of Tortonian
362 strata (20°SE) indicate that strike-slip deformation occurred before the deposition of Tortonian conglomerates and
363 after the tilting of the NF foliation (see cross section in **Fig. 10a**). This argues that the transition from HP
364 metamorphism (Burdigalian-Langhian) in the NF (Platt et al., 2006) to W-directed ductile crustal thinning and right-
365 lateral strike-slip faulting occurred before the Tortonian, most likely around the Serravallian at 12-13 Ma. This interval
366 is considered to mark the transition from ductile to brittle extension in the region (e.g. Augier et al., 2013). Because
367 strike-slip faulting postdates folding of the NF foliation, and are consistent with WSW-ENE oblique extension, we
368 suggest that the Sierra de los Filabres metamorphic dome formed in a transtensional strain regime. This hypothesis
369 conforms with prediction of transtension at the tip of the STEP fault (Le Pourhiet et al., 2012) and with model of
370 oblique extension (see **Fig. 3**).
371

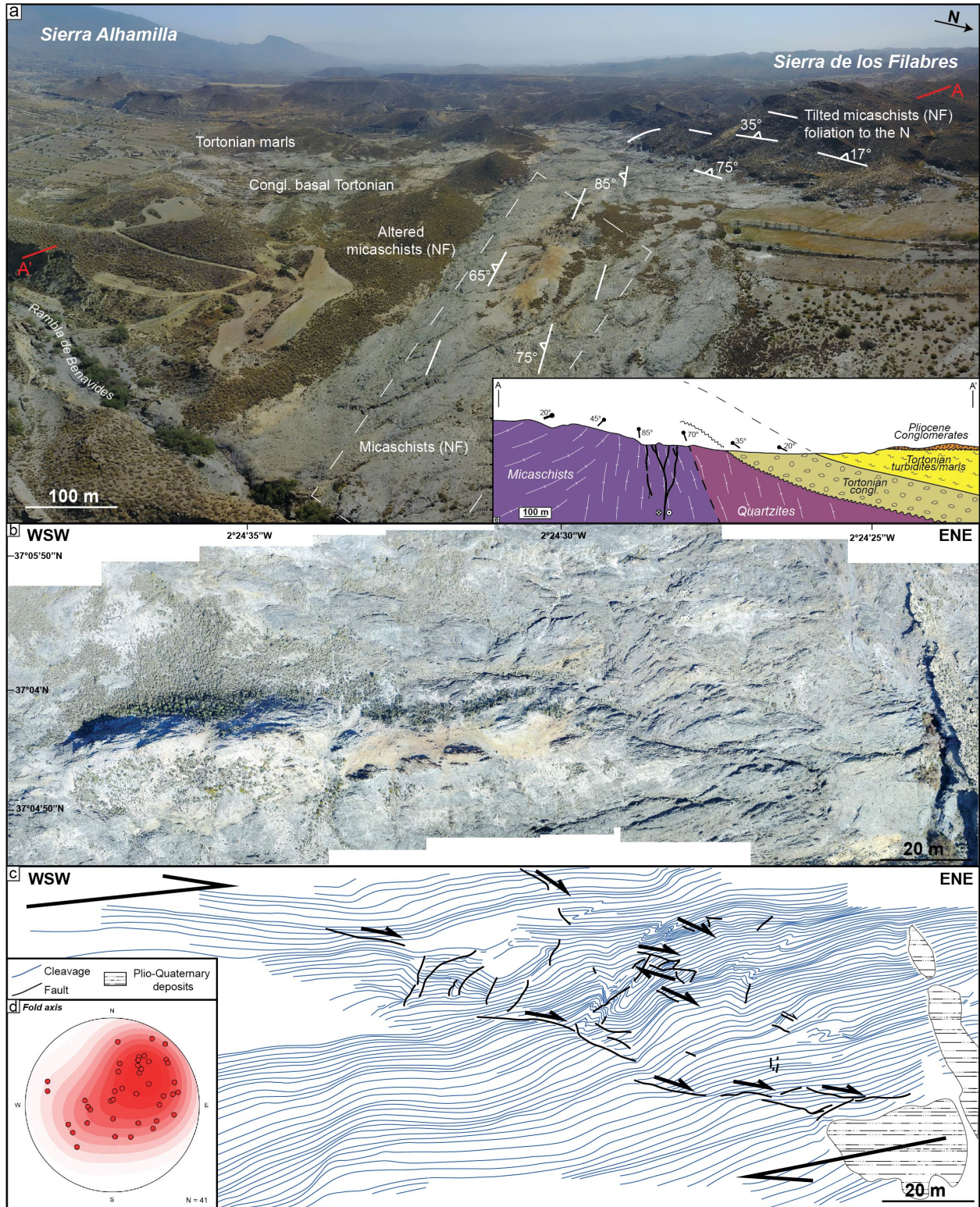


372
 373 **Figure 9.** (a) and (b) Fault zone at the contact between the Tortonian basal conglomerates and the series of the
 374 Alpujarride complex south of AC (Rambla de Tices, see Fig. 5 for location). (c) slickensides on the fault zone reveal
 375 a normal sense of slip with right-lateral strike-slip component found in association with (d) cataclastic breccias,
 376 sheared boudins of metamorphic and sedimentary rocks. Al-d: Alpujarride dolomites; bT-cCg: basal Tortonian
 377 continental Conglomerates; PI-Cg: Pliocene Conglomerates. Coordinates 37.031944°N/-2.716274°E.
 378

379 4.3. NW-SE-trending normal faults

380 A second set is represented by NW-SE directed normal faults (Fig. 8). They are found, for instance, bordering the the
 381 NE part of Alhabia basin, where they cut across the basement and interrupt the westward continuity of the southern

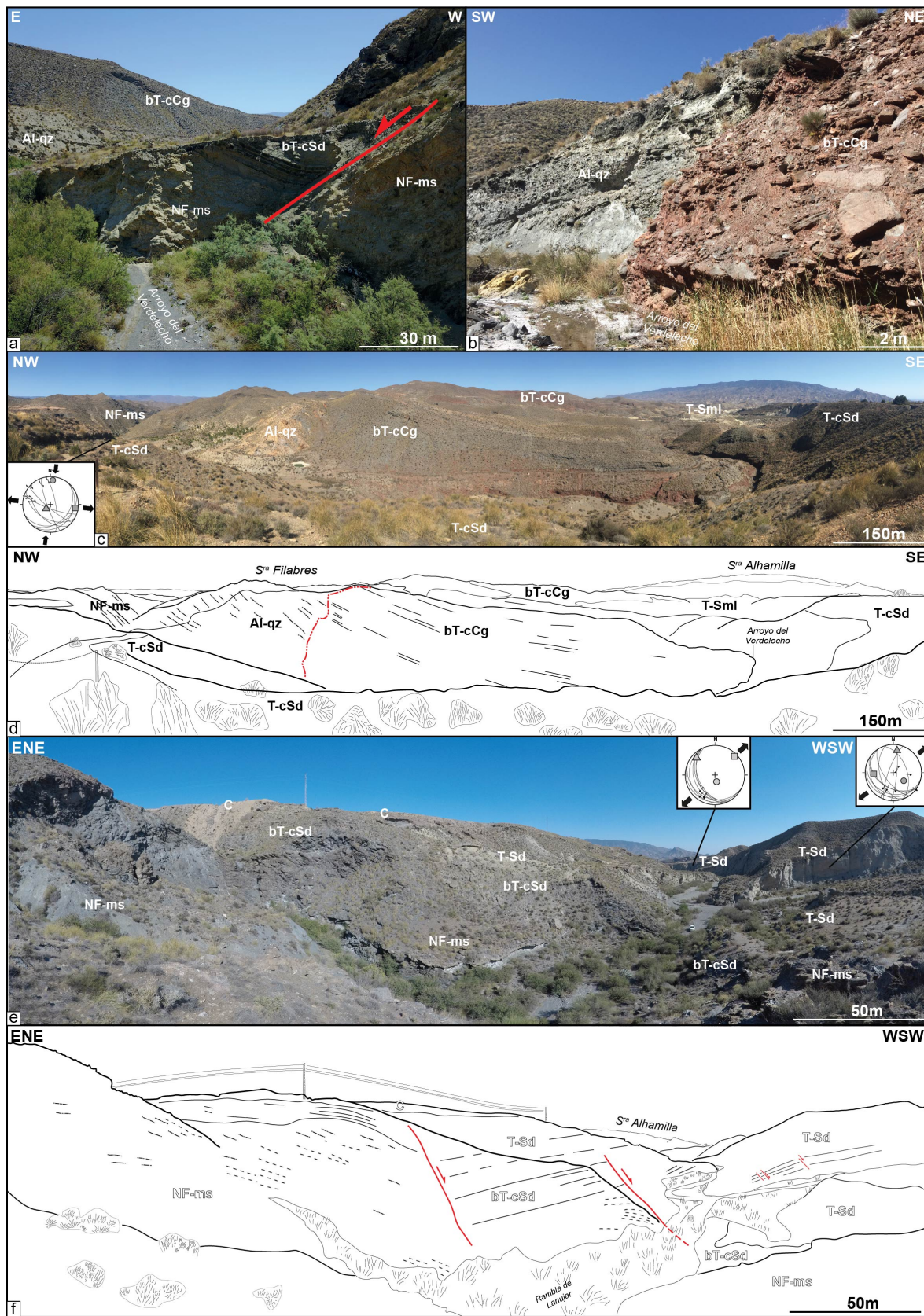
382 flank of the Sierra de los Filabres. One major fault zone of this system is well exposed in the Arroyo del Verdelecho,
383 7 km to the west of Tabernas, on the eastern border of the Alhabia basin (**Figs. 11 and S2**). From a regional point of
384 view this large NW-SE fault zone controls the deepening of the Tortonian basin and the position of Pliocene
385 depocenter in its hangingwall, towards the West. NW-SE normal faults also cut across the lower Tortonian
386 conglomerates in the hangingwall but their throw diminishes upward in the upper Tortonian margin sediments,
387 suggesting fault activity during the late Tortonian (**Fig. 11**). One major fault zone is outlined by cataclastic breccias
388 made of marbles originated from the exhumed Alpujarride complex in the Sierra de los Filabres (**Fig. S2**).
389 South of HOB (south of Arboleas), NW-SE faults are seen cutting through the late Tortonian sands and marls series,
390 indicating that NE-SW extension is at least Tortonian (**Figs. S1c, d**).
391



392
393
394
395
396
397

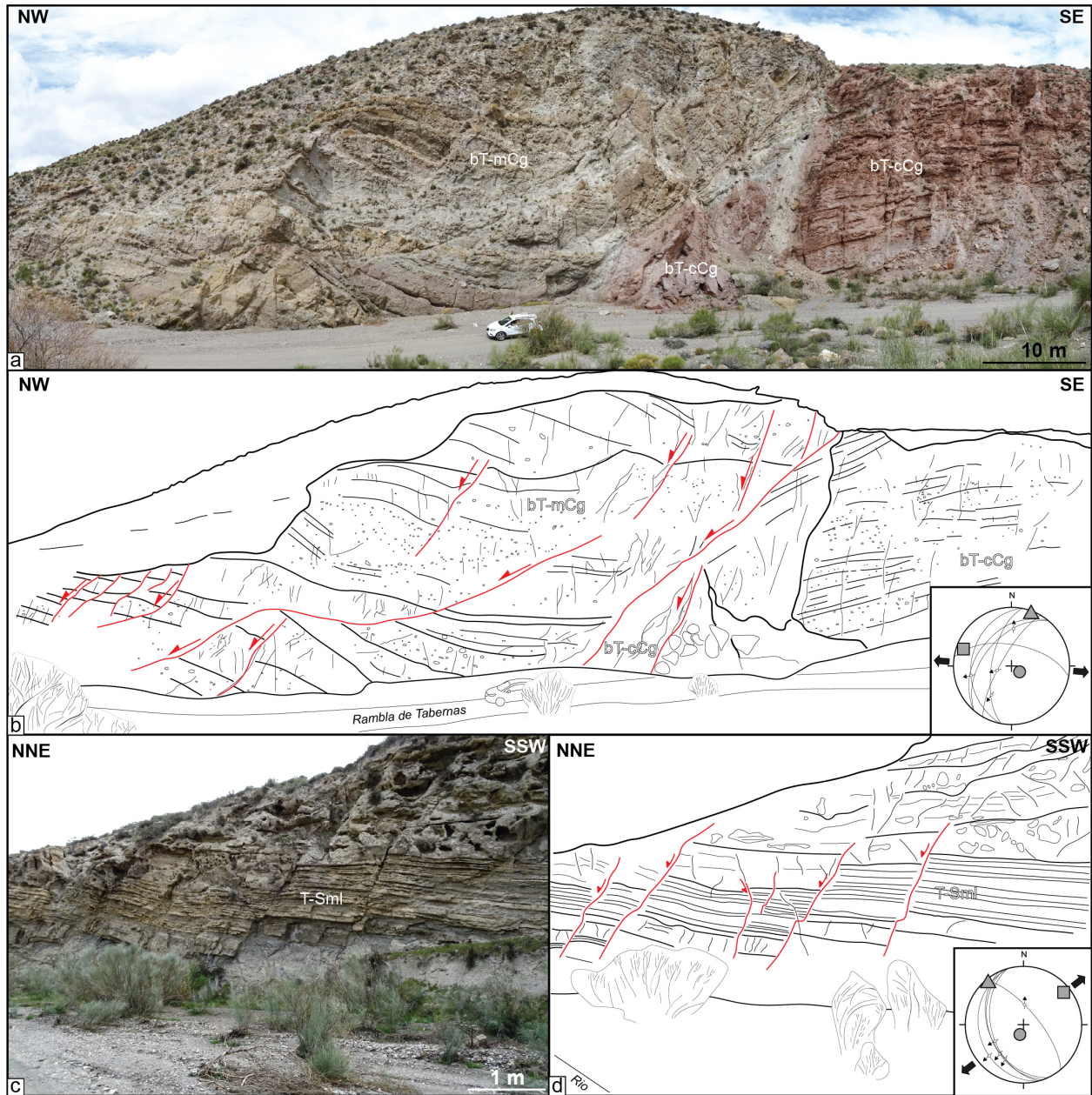
Figure 10 : (a) Drone view taken in the SSW direction of the southern flank of the Sierra de los Filabres at the contact with the Tabernas basin (see Figure 5 for location). Local folding of the micaschist is apparent in the right where the foliation is striking NNE-SSW and is dipping $\sim 25^\circ$ E whereas it is vertical and striking SW-NE in the center of the studied area forming paleosurface. Local cross section highlights the unconformable contact between the Tortonian conglomerates and overlying on the basement. (b) High-resolution drone images of the paleosurface and (c) line-

398 drawing of the foliation revealing secondary folding (see **(d)** stereoplot of fold axes inclined to the NE) and dextral
399 shear zones. Coordinates 37.082777°N/-2.410544°E.
400
401
402



404 **Figure 11** : (a) Field photographs of a NW-SE normal fault at the contact between the Nevado-Filabride micaschists
405 (footwall) and Tortonian sediments (hanging wall). (b) Stratigraphic contact between grey and red basal Tortonian
406 continental conglomerates. These thick Tortonian series rest conformably on the Alpujarride complex (c, d).
407 Coordinates 37.059507°N/-2.478386°E. (e, f) NW-SE normal faults cutting across the NF micaschists basement.
408 These faults that also affect the early Tortonian deposits are sealed by late Tortonian deposits and are therefore syn-
409 depositional. See Figure 5 for location. Al-qz: Alpujarride quartzites; NF-ms: Nevado-Filabride micaschists; bT-cCg:
410 basal Tortonian continental Conglomerates; bT-cSd: basal Tortonian continental Sandstones; T-cSd: Tortonian coarse
411 Sandstones; T-Sd: Tortonian Sandstones; T-Sml: Tortonian Sandstones-marls; C: calcretes. Coordinates
412 37.061279°N/-2.490309°E. Paleostress orientations are in Table S1.
413

414 Both fault slip data and our own observations argue for a regional pre-Tortonian and syn-early Tortonian NNE-SSW
415 directed extension. This direction of extension is also found associated with less well-developed strike-slip regimes
416 (Fig. 8). It is consistent with the D1-D2 phase of brittle deformation found in HOB (Augier et al., 2013). The fact that
417 extension and strike-slip regimes occurred synchronously, or overlap rapidly in time, supports the view that they
418 reflect the same large-scale tectonic setting. The reason why strike-slip faulting is less apparent in the field than
419 expected in models in Fig. 3 is likely to reflect the fact that oblique extension is not fully partitioned between normal
420 and strike-slip components and is actually distributed along oblique structures. Moreover, where strike-slip faults are
421 found they are associated with narrow basins or near the contact between the cover and basement but not in the center
422 of HOB or TB. The NNE-SSW to NW-SE faults appear to postdate the deposition of the early Tortonian red
423 conglomerates and is synchronous with the deposition of marine Tortonian series (Fig. 12). These normal faults
424 currently form half-graben filled with Plio-Quaternary deposits (Guadix, Baza, Alhabia) and are active today. But the
425 importance of extension-related brittle deformation over brittle compression decreases eastwards. Indeed, a late brittle
426 compressional event oriented roughly N-S is described in the literature as a D3 brittle event (e.g. in HOB) associated
427 with reverse and strike-slip faults (Augier et al., 2013). The post-late Tortonian shortening is seen responsible for fold
428 amplification and reverse faulting on the northern limb of Sierra de Alhamilla and Sierra de los Filabres, and locally
429 in the eastern part of the HOB near the termination of left-lateral strike-slip faulting evolution of the Alhama de Murcia
430 fault (Fig. 8).



431
 432 **Figure 12:** (a, b) N-S to NNE-SSW-oriented normal to dextral faults affecting the basal Tortonian continental
 433 conglomerates (bT-cCg) and marine conglomerates (bT-mCg) (Rambla de Tabernas). They form a long and tight E-
 434 W anticlinal crosses the Tabernas basin (see Figure 5 for location). (c, d) Several normal faults observed in Tortonian
 435 sandstones and marls (T-Sml). They are mostly oriented NNW-SSE. Coordinates 37.041648°N/-2.399318°E.
 436 Paleostress orientations are in Table S1.

437 **5. N-S crustal-scale section across the oblique/transform margin of Alboran basin**

438 To examine further the structural relationships between extension and strike-slip faulting across the Alboran margin,
 439 we explore 2D multichannel seismic lines acquired during the MARSIBAL 1-06 cruise (Comas and MARSIBAL1-
 440 06 Scientific Party, 2007) and ESCI cruises (Comas et al., 1995) across the Eastern Alboran basin (EAB). The studied
 441 seismic dataset consists of ~300 km and are deep-penetration multichannel seismic reflection studies (12 s two-way
 442 travel time - TWTT). Here, we study two lines namely MSB08 and MSB07 (see location in Fig. 1). For stratigraphic

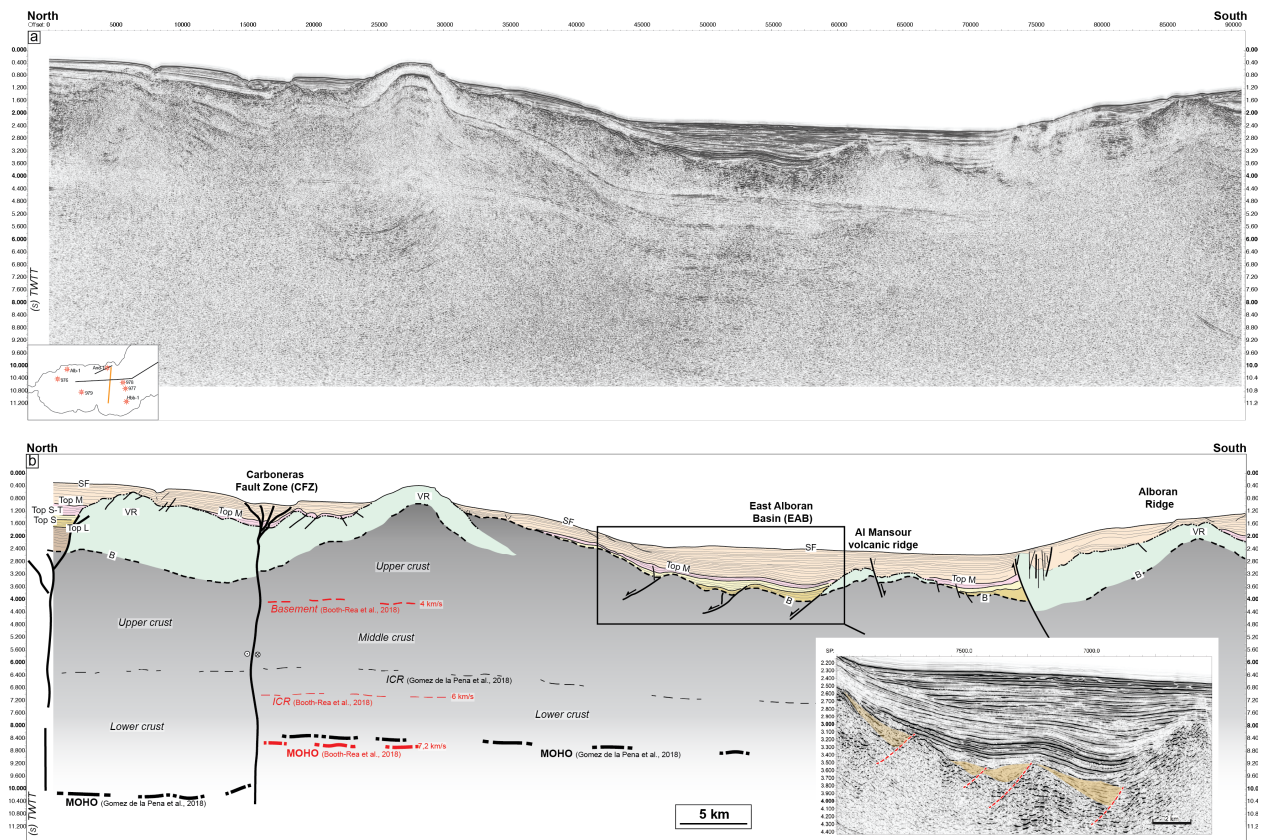
443 and structural correlations between the studied seismic lines, we used the Andaluçia-A1 well (**Fig. 6a**) and results
 444 from ODP 977 and 978 legs (see location in **Fig. 1**). MSB08 is striking N70°E, slightly oblique to the shoreline. It is
 445 close, and runs parallel, to TM08 line of Gómez de la Peña et al. (2018). It is calibrated by Andaluçia-A1 well and
 446 ESCI-Alb1 line (Comas et al., 1995). Line MSB07 stretches in the N-S direction between the EAB in Spain and SAB
 447 to the north of Morocco parallel to line TM09 (Gómez de la Peña et al., 2018) and crosscuts line ESCI Alb2b
 448 presented in Comas et al. (1995) and Booth-Rea et al. (2007) (**Fig. 1**).

449

450 5.1 Offshore structures and stratigraphic architecture

451 The Carboneras Fault is well imaged north of MSB07 (**Fig. 13**). It forms a negative crustal-scale flower structure
 452 related to left-lateral strike-slip faulting that involves a Moho depth variation between 12 s to 9-8 s TWT after Gómez
 453 de la Peña et al. (2018). It separates a thin continental crust to the North (25-20 km; **Fig. 2**), from the magmatic calc-
 454 alkaline arc crust of the EAB with a thickness of 18 km in the south (Booth-Rea et al., 2007, 2018; Gómez de la Peña
 455 et al., 2018, 2020a).

456



457

458 **Figure 13** : Seismic reflection line MSB07 (location on **Fig. 1**). Discontinuous intracrustal reflectors (ICR) imaged
 459 between 3 and 6.5 s TWT, have been interpreted as mylonitic zones within the metamorphic basement (Carbonell et
 460 al., 1998; García-Dueñas et al., 1994; Gómez de la Peña et al., 2018). VR: Volcanic Ridge; B: Acoustic basement;
 461 Top L : Top Langian; Top S: Top Serravallian; Top S-T: top Serravallian-Tortonian; Top M: Top Messinian; SF:
 462 Seafloor.

463

464
465
466
467
468
469
470
471
472
473
474
475
476
477
478
479
480
481
482
483
484
485
486
487
488
489
490
491
492
493
494
495
496
497
498
499
500

Reflection seismic data (**Figs. 13, 14, 15**) collectively show a stratified crust, corresponding to the sediment cover, down to 2.4-4 s TWT, which outlines the acoustic basement with high reflectivity (B). Locally, the top basement reflector coincides with erosional palaeo-relief or high angle normal faults bounding basement highs. These faults are oriented mostly NW-SE to NE-SW and cut across the basement. We recognized on seismic images magmatic additions in the continental crust that are shaped by volcanic edifices exposed on the seafloor (e.g. Chella Bank) or slightly buried (Alboran Ridge) outlined by symmetric downlaps and onlaps of sediments. These constructions form topographic highs such as the Chella Bank on the MSB08 line (**Fig. 14**), the Alboran Ridge on the MSB07 line (**Fig. 13**) and the Maimonides Ridge on the ESCI-Alb2b line (**Fig. 15**). All the reflectors corresponding to layers as old as Tortonian are onlapping against the volcanic ridges confirming that the volcanic activity occurred during the middle to late Miocene times, which is shown by Duggen et al. (2008). Some reflectors up to the top Messinian (top M) onlap onto the volcanic ridges probably as a result of Pliocene uplift.

The stratigraphy offshore, on the continental crustal domain, is defined by the recognition of five seismic stratigraphic units in Andalucía-A1 well (Jurado and Comas, 1992) labeled I-V from top to base (**Figs 6 and 16**) and separated by unconformities. The seismostratigraphic units I to V vary in thickness (**Fig. 16**) and their architecture is conditioned by the occurrence of basement highs and crustal-scale faults.

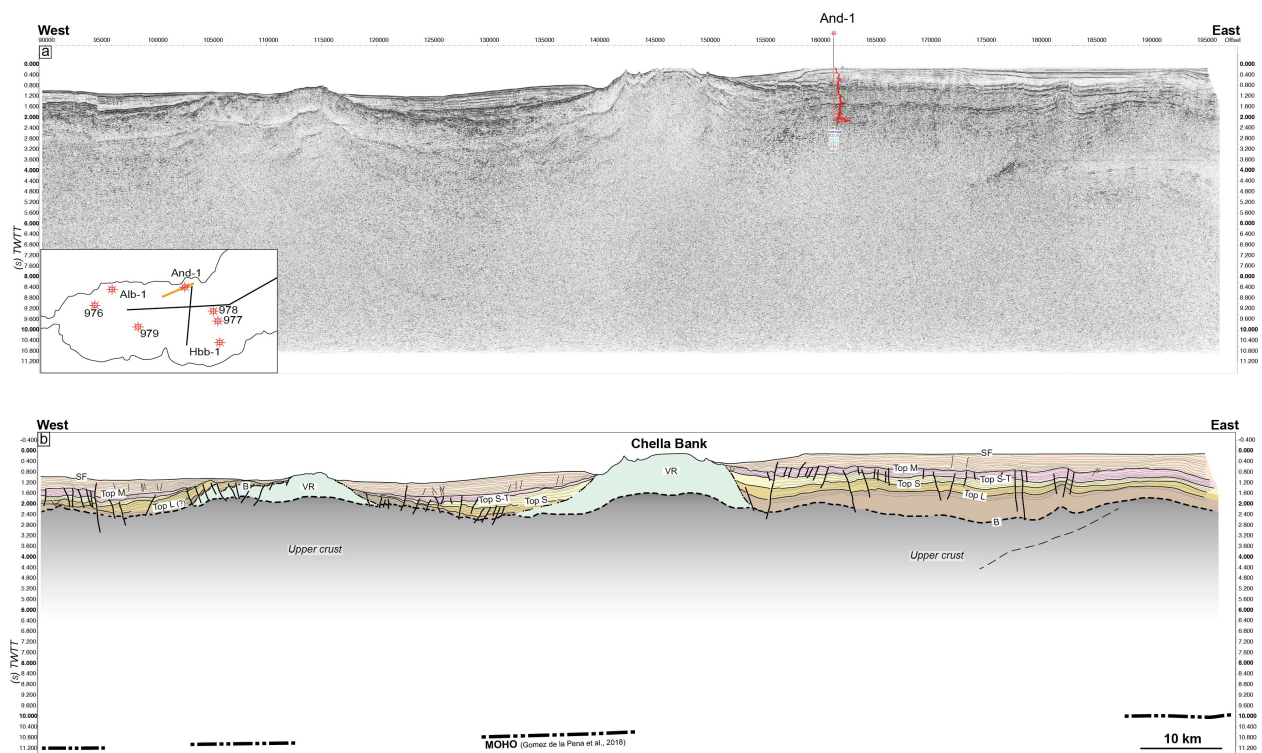
Below the Miocene sedimentary filling, Andalucía-A1 well reveals ~190m of phyllitic and quartzitic meta-sediments (2.4 to 4 s TWT below the Alboran basin, **Figs. 13 and 14**) topped by Langhian to Tortonian marls (top at ~1.6 to 3.4 s TWT below the Alboran basin) interbedded with Tortonian-Messinian tuffs and basaltic lavas. These units have been correlated in the magmatic arc crust of EAB after Gómez de la Peña et al. (2020b). The older deposits (Unit V) Langhian-Serravallian in age, consist of clays and marls with intercalated sands and volcano-clastic deposits. The seismic facies of this Unit V is made of moderate amplitude and low frequency discontinuous reflections packages (**Figure 16**), and is only present in the Northern Alboran Basin. They are correlated with volcanic series in the EAB (vY3) (Gómez de la Peña et al., 2020b). They pass upward into Serravallian sand-silty clay turbidite (Unit IV) possibly correlated with volcanic series in EAB (vY2 after Gómez de la Peña et al., 2020b). This unit exhibiting low to moderate amplitude, moderate frequency drawing continuous sheeted to disrupted reflectors, is unconformably overlying Unit V and locally onlaps onto the basement. Thickness of Unit IV remains rather thin in the North and East Alboran Basin. It can't be properly identified in the South Balearic Basin, east of the Maimonides volcanic ridge (**Fig. 15**). The Unit III dated from late Serravallian to late Tortonian is represented by sandstones interbedded with volcano-clastic levels which correlates in EAB with volcanics vY1 unit. Unit III contains internal reflections characterized by low to moderate amplitude, moderate frequency continuous sheeted reflectors. Its thickness remains relatively constant from the NAB to the EAB, and is identified beneath the Messinian Unit II in the South Balearic Basin. Unit II corresponds to the Messinian evaporite, carbonate, volcanic, and volcanoclastic deposits interbedded with fine-grained sediments and is equivalent to unit III of Gómez de la Peña et al. (2020b) in EAB. Seismic facies of Unit II is marked in the Alboran domain by lower amplitudes and lower frequency reflectors. In ESCI-Alb2b line, Unit II increases drastically east of the Maimonides ridge, which delimits the western boundary of the salt deposits in the Western Mediterranean basin

501 during the Messinian Salinity Crisis (Haq et al., 2020). Unit II is topped by Unit I made of Pliocene to Quaternary
 502 clays and sanstones, which are correlated with units II and I in EAB (Gómez de la Peña et al., 2020b). Unit I is marked
 503 by thinly bedded, mostly parallel, high-frequency and low amplitudes reflectors (**Fig. 15**). Its thickness fluctuates in
 504 response to sedimentary processes (Juan et al., 2016).

505 Along line MSB08 (**Fig. 14**) the Langhian-Serravallian (Unit V) is maximum 1600 m-thick (using a P-wave velocity
 506 of 3.2 km/s calculated within Andalucia-A1 well). In EAB, south of Carboneras Fault Zone, the total thickness of Unit
 507 V is only ~300 m on MSB07 (**Fig. 13**) and is absent in ESCI-Alb2b (**Fig. 15**). The Serravallian-Tortonian (Unit IV-
 508 III) interval shows only very limited sediment accumulation (~300 m) except near the NW-SE oriented normal faults
 509 where growth geometries are visible. These normal faults are sealed by the Tortonian-Messinian deposits, indicating
 510 a syn-sedimentary faulting during the middle Miocene (**Fig. 13**). With respect to onshore observations this
 511 sedimentary infill is more continuous and is also much thinner compared to TB and HOB where they are represented
 512 by thick conglomerates and marls/turbidites (> 1km) (**Fig. 7**), and they are eroded or not deposited along the axes of
 513 the metamorphic domes. The Messinian deposits (Unit II) are ~150-350 m-thick north of CF (MSB07-08 ; **Figs. 13,**
 514 **14**) and increase to about 1200 m eastward in the eastern EAB (ESCI-Alb2b ; **Fig. 15**), and in Algero-Balearic basin
 515 (Gómez de la Peña et al., 2020b). The top Messinian reflector is topped by thick horizontal sedimentary strata, with a
 516 maximum thickness of 1.2 s TWT (~2.4 km assuming a velocity of 2 km/s) on line MSB07, suggesting an important
 517 channel system during the Pliocene.

518 The Pliocene-to-Quaternary series are poorly deformed except in the vicinity of CF and near the Alboran Ridge where
 519 this is associated with south-dipping reverse fault (**Fig. 13**). This late and still active compressional tectonics is
 520 revealed by the overthrusting of the SAB over the south margin of the EAB (e.g. Martínez-García et al., 2011).

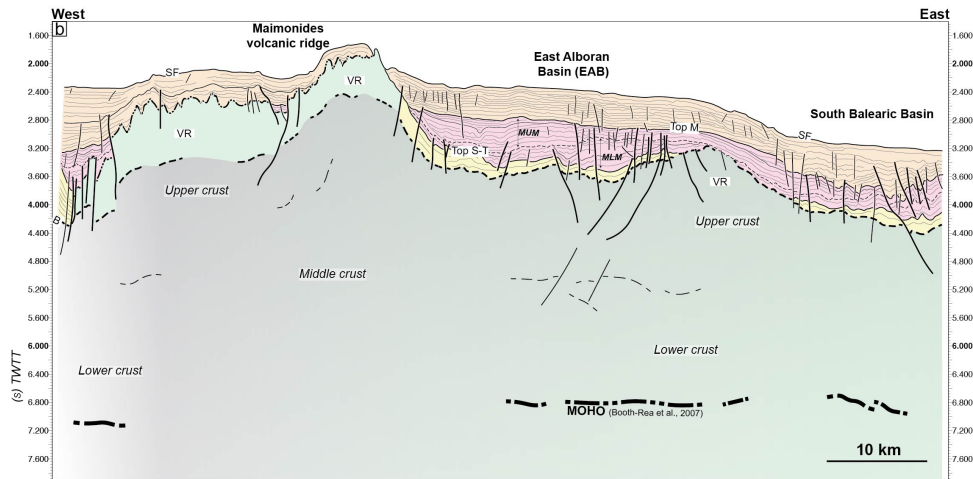
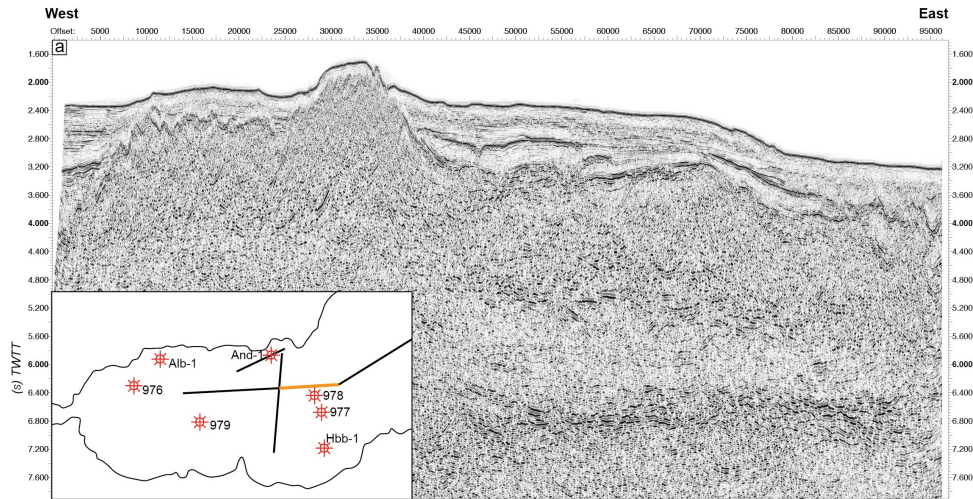
521



522

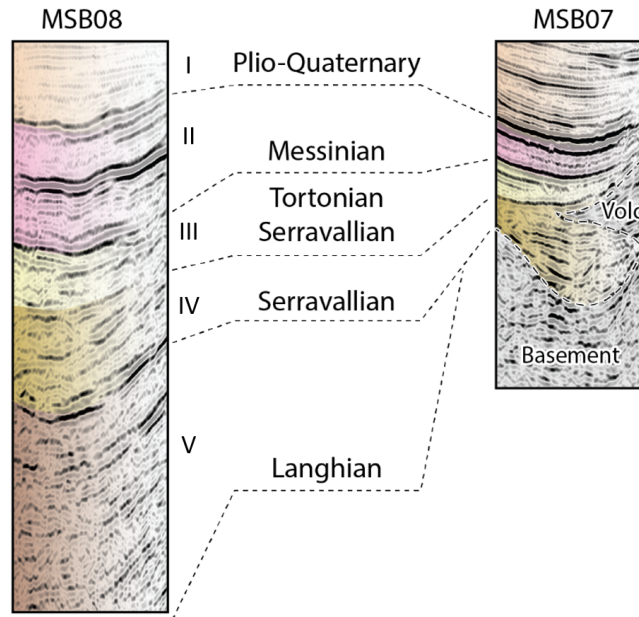
523
524
525

Figure 14 : Seismic reflection line MSB08 (see location on **Fig. 1**). See Figure 13 for abbreviations. See also Figure S3 showing a zoom on the main seismic facies recognized in Andaluca-A1 well.



526
527
528
529
530

Figure 15. (a, b) Seismic reflection line ESCI-Alb2b and interpretation (see Figure 1 for location). Seismic units are correlated with those defined by Booth-Rea et al. (2007). See Figure 13 for abbreviations.

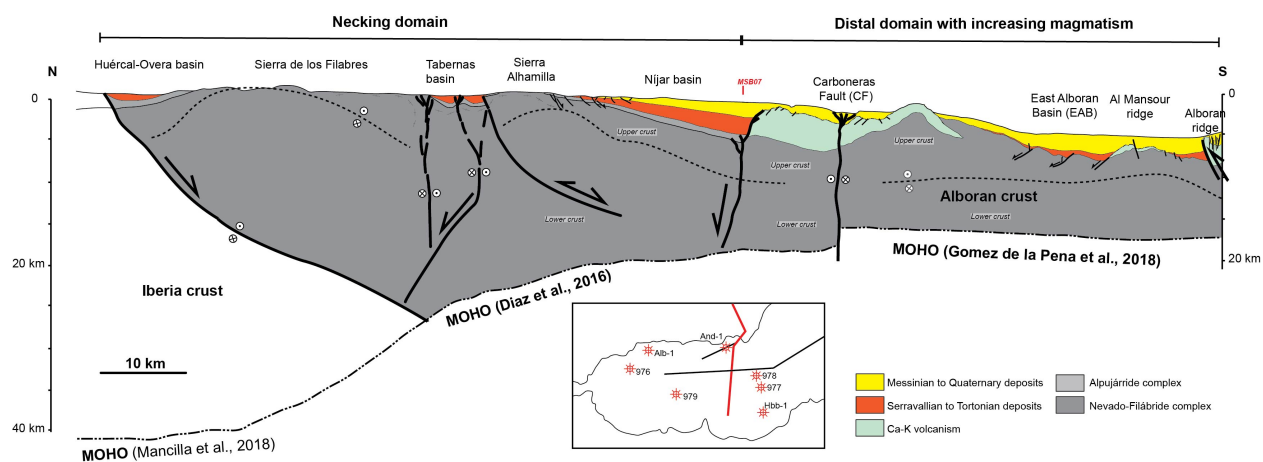


531
 532 **Figure 16** : Seismic facies of units I to V seen through seismic lines MSB08 close to the shoreline and the line
 533 MSB07, located deeper in the East Alboran Basin.

534 **5.2 N-S crustal cross-section of the Alboran margin accounting for strike-slip faulting**

535 Based on subsurface constraints and field data, we present in **Figure 17** a crustal-scale section across the rifted margin,
 536 from the Sierra de las Estancias and Huerca-Overa basin (HOB) to the Alboran ridge that represents the inverted
 537 southern margin of the EAB. The proximal margin, where the crust is 30-35 km-thick, is defined to the North by the
 538 transition between the south Iberia margin, and the metamorphic domain of the Alboran basement exposed in the
 539 Sierra de las Estancias. This continental domain preserves part of the crustal thickness acquired during former Betic
 540 orogenic phase that has been little involved in crustal thinning. The onset of crustal thinning to the south coincides
 541 with the position of the lithospheric tear fault documented by seismology (**Fig. 4**; Mancilla et al., 2015a) and is
 542 recorded by the formation of asymmetric basins of the HOB and TB, shaping the upper neck domain. Orthogonal and
 543 oblique extension in this domain is accommodated by normal and strike-slip faulting during the Tortonian. From the
 544 Sierra de los Filabres to the south, the thickness of the continental crust reduces to 25 km in the Tabernas basin along
 545 the Alpujarras strike-slip fault zone and below the Sierra Alhamilla (**Fig. 17**). The Nijar basin depicts the transition
 546 towards offshore distal domains where the continental crust reaches a thickness of 20 km. The Tortonian and
 547 Messinian marine sediments are also thicker. It is worth noting that a number of volcanic bodies offshore (e.g. Chella
 548 Bank on MSB08) accompany crustal thinning of the continental crust. The Carboneras Fault (CF) brings crusts with
 549 different thicknesses and composition into contact. South of CF, the crustal thickness of the EAB is 18 km and seismic
 550 velocities, especially the occurrence of a high- V_p lower crust, has been considered to indicate the EAB is floored by
 551 a magmatic arc crust (Gómez de la Peña et al., 2018; 2020), formed in a supra-subduction context above the subducting
 552 Alboran slab (Booth-Rea et al., 2018). The crustal thickness of the EAB is compatible with crustal thinning of the
 553 continental margin, and the occurrence of NW-SE-trending faults also recognized onshore despite being slightly older
 554 (Serravalian-Tortonian) suggest that the EAB formed under the same back-arc extension setting, relative to westward

555 slab retreat as the whole Alboran margin did. Thus, the magmatic arc crust of the EAB could represent voluminous
 556 magmatic intrusions (e.g. Al Mansour dacite, Alboran Ridge rhyolite dated to ca. 9 Ma; Duggen et al., 2004; Tendero-
 557 Salmerón et al., 2022; **Fig 17**) formed on the distal rifted margin of Alboran. The investigation of the causes of calc-
 558 alkaline magmatism is beyond the scope of this study, but we suspect it reflects post-subduction arc magmatism
 559 induced by remelting, during extension and delamination, of a metasomatized wedge of mantle lithosphere formed
 560 during a previous subduction event (e.g. Richards, 2009). The fact that calc-alkaline magmatism around 10 Ma that is
 561 10 to 5 myrs after the onset of upper plate extension in the Betic-Alboran region supports this view. Note that in
 562 contrast to Gómez de la Peña et al. (2020) and Booth-Rea et al. (2018) we implicitly assume the magmatic arc crust
 563 of EAB is not a newly formed crust but rather represents a thinned continental crust later intruded by calc-alkaline
 564 magmas. Different crustal domains are expected across a rifted margin that has involved variable amount and types
 565 of mantle-derived magmatism, especially if delamination/subduction occurred during extension. The observation of
 566 contrasting types of crustal domains now juxtaposed in the NS direction is also related to the fact that extension is
 567 oriented perpendicular to the section.
 568 Crustal shortening in **Figure 17** is distributed across north-vergent reverse faults below the Alboran Ridge, on the
 569 northern limb of Sierra de Alhamilla, and CF strike-slip fault zone.



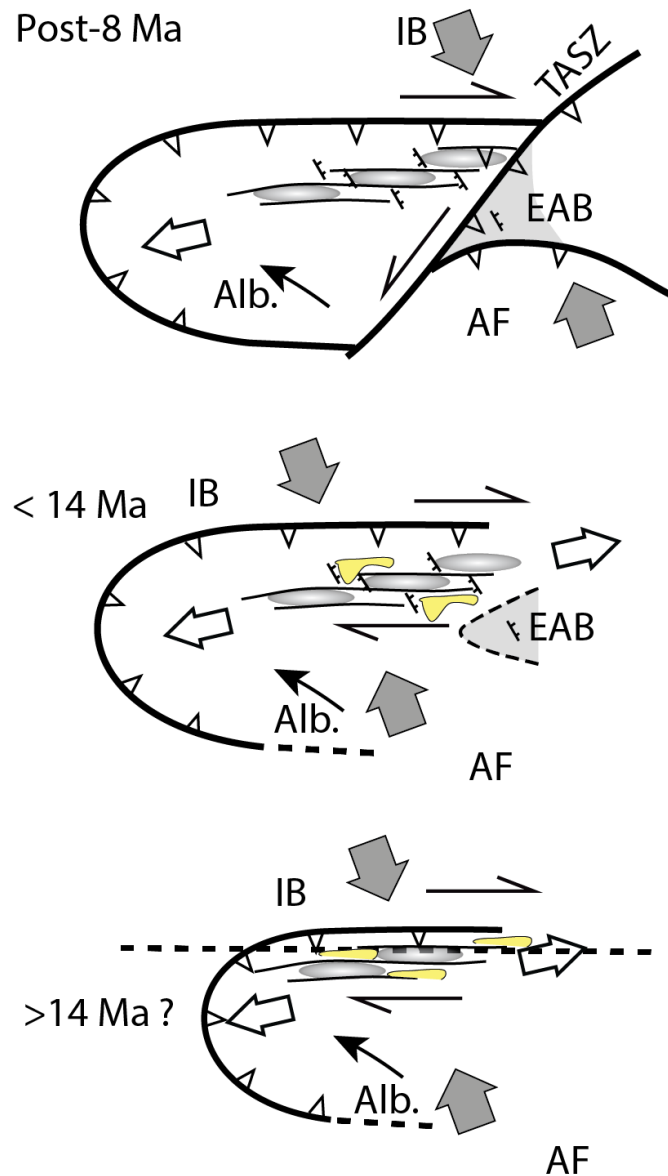
570
 571 **Figure 17.** Crustal-scale cross section of the Alboran margin in the eastern Betics interpreted based on onshore and
 572 offshore constraints presented in the text. Note that in the necking domain the extension of faults downwards to
 573 Moho depths is not imaged on the seismics and therefore largely inspired by inferences from 3D numerical models
 574 (see Fig. 3).
 575
 576

577 **6. Implications**

578 The question of whether the Miocene tectonic evolution of the Betics reflects crustal thinning associated with oblique
579 back-arc rifting as suggested from present-day strain patterns is unclear in the literature. We found based on a
580 comparison between numerical models and basin analyses, fault kinematics and structure of the margin in the eastern
581 Betics compelling evidences that crustal thinning was controlled by oblique extension. Oblique rifting operated since
582 at least the middle Miocene in relation with Alboran slab retreat below the Alboran basin and is kinematically
583 associated with slab tearing and delamination below the central and eastern Betics.

584 One of the most striking tectonic feature of the Alboran margin (**Fig. 17**) is the abrupt N-S crustal thinning oblique to
585 the direction of slab rollback. The history of sediment infill and rates of subsidence in intramontane basins (**Figs. 6**
586 **and 7**) combined with the analyses of fault slip data (**Fig. 8**), and structural data offshore (**Fig. 13**), confirm that brittle
587 extension oriented from N20°E to EW occurred during an interval spanning from the Serravallian-early Tortonian to
588 the late Tortonian (14-8 Ma) (**Fig. 18**). This extension is found associated with both normal and strike-slip regimes.
589 Field tectonic data reveal that N20°E extension is more represented in HOB while the ENE-WSW to EW extension is
590 found related with the evolution of the Almanzora fault zone, Alpujarras fault zone and Tabernas basin flanking the
591 metamorphic domes (**Table S1**). There are additional evidence that EW-directed dextral strike-slip faulting occurred
592 during the Tortonian to the South and West of the HOB. These large-scale transfer fault zones positioned on the slab
593 edge accommodate the differential westward extension that are later cut by Tortonian NW-SE faults. These second
594 set of faults is also observed in the magmatic crust of the EAB offshore but seismic data indicate they are Serravallian-
595 Tortonian in age and therefore older than those identified onshore. We suggest that NW-SE normal faulting could
596 have initiated in the EAB then migrated towards the necking domain as slab retreat progressed and the width of the
597 region affected by crustal thinning widened (**Fig. 18**). Subsidence during the Serravallian-Tortonian appears to have
598 been lower in the EAB compared to intramontane basins onshore. This suggests that the isostatic effect of crustal
599 thinning was compensated by a thermal anomaly in the mantle, heralding the Ca-K magmatism at 11-7 Ma (Duggen
600 et al., 2004, 2008).

601



602

603 **Figure 18:** Tectonic model of the evolution of the northern margin of the Alboran Rift. Large grey and white double
 604 arrows depict shortening, which is parallel to the AF/IB convergence, and the highly oblique extension, respectively.
 605 The thin black arrows show the motion of Alboran relative to Iberia (IB) taken from Figure 4. Half arrows depict
 606 distributed strike-slip faulting in the Betics. NW-SE directed normal fault and strike-slip basins (yellow) are
 607 consistent with the oblique extension. Grey-shaded ellipses represent the metamorphic domes. TASZ : simplified
 608 representation of the Trans-Alboran Shear Zone. We also indicated EAB which mostly formed ca. 9 Ma (Duggen et
 609 al., 2004; Booth-Rea et al., 2018).

610

611 Several key tectonic features found in the eastern Betics are predicted by 3D models of oblique extension (**Figure 3**).
 612 They include E-W trending normal faults that are prevalent on the upper neck domain (i.e. Sierra de las Estancias and
 613 HOB), and E-W strike-slip faults (Almanzora and Alpujarras fault zones). NW-SE normal faults are associated with

614 more distal domains on the continental margin where crustal thinning is the highest offshore, south of Nijar basin, and
615 in the EAB.

616 Tectonic inversion seems, in contrast, to have been increasingly more important when approaching the Carboneras
617 and Palomares strike-slip faults in the East since the late Tortonian.

618 Ductile thinning associated with the formation of metamorphic domes and exhumation of HP rocks is dated to 23 to
619 16 Ma (Platt et al., 2003; Booth-Rea et al., 2015). This provides time constraint for the beginning of oblique extension
620 and westward slab rollback. Deformation at the future location of the tear fault was probably initially diffuse and
621 resulted in an immature oblique rift system in the South, combined with thrusting in the external zones to the North
622 (**Figure 18**). In the Serravallian (14-13 Ma), accompanying slab steepening, localization of slab tearing, and
623 propagation of thrusting in external zones, oblique extension spread over the whole central Betics. At this time,
624 metamorphic domes exhumed to upper crustal levels (e.g. Vázquez et al., 2011) and recorded the transition from
625 ductile shearing to brittle faulting (**Figure 18**). Brittle E-W-directed stretching and dextral transcurrent deformation
626 formed at this time. The late/post-Tortonian times (from 10-8 Ma) marks a change in the tectonic evolution of the
627 Betics and Alboran domain possibly related to the onset of slab detachment in the eastern Betics (van Hinsbergen et
628 al., 2014; Do Couto et al., 2014; Mancilla et al., 2015a; Martínez-García et al., 2017; d'Acremont et al., 2020; García-
629 Castellanos and Villaseñor, 2011; Spakman et al., 2018). This event is synchronous with the indentation by the
630 magmatic arc crust of the EAB in the Águilas Arc (Ercilla et al., 2022), amplification of the metamorphic domes in
631 the vicinity of the EBSZ (e.g. Alhamilla), transition from Ca-K in EAB to more alkaline magmatism in eastern Betics,
632 and at the regional scale with exhumation in northern Iberia (Rat et al., 2022) and N-S shortening in northern Africa
633 (Jolivet et al., 2021a) (**Figure 18**).

634 In this model, ductile stretching and ductile detachment associated with the development of the domes are the
635 expression of oblique E-W extension. It provides a coherent scheme linking the formation of EW-directed basins in
636 the brittle field associated with strike-slip faulting, and NW-SE/NNW-SSE sedimentary basins (Guadix, Baza,
637 Alhabia) formed in transtension during the Tortonian. As such, the oblique extension is closely associated with STEP
638 faulting required by westward slab rollback. The oblique rifting model we propose explain the formation of the
639 metamorphic domes and intermontane basins and provides insight into crustal deformation, which is broadly
640 consistent with the geodynamic models of slab rollback and tearing since 20 Ma that have been previously proposed
641 for Alboran (Chertova et al., 2014; Spakman et al., 2018). In the latter models, however, the ENE-WSW extension in
642 the central-eastern Betics is related to differential absolute motions between Iberia and the slab decoupled from Iberia
643 by slab tearing. In our scenario, oblique extension is entirely related to westward lateral rollback. It can not be
644 excluded, however, that the effect of mantle-derived slab dragging increased during the late extensional stage, from
645 14-13 Ma, when slab tearing localized.

646 Mid-Miocene high-pressure metamorphism documented in the central Betics (e.g. Platt et al., 2013) was synchronous
647 with slab steepening and subduction that was under way during oblique back-arc extension (**Figure 18**). The case of
648 exhumation of high-pressure rocks in oblique convergence setting associated with near-parallel orogen extension is
649 also documented in other active orogen like Taiwan (Conand et al., 2020).

650 This highly oblique northern Alboran margin differs from typical transform fault margin such as those associated with
651 the Atlantic ocean because it accommodates variations in intra-plate extensional movements, triggered by slab roll-
652 back, not variations in spreading rates. Strike-slip faults may have originated as low-angle normal faults which were
653 later reactivated as thrusts during margin inversion. Similar observations, including metamorphism, strike-slip
654 faulting, high geothermal gradients and volcanism has been made in Seram, north of the Banda Arc, which represents
655 another example of extremely thinned crust formed perpendicular to the direction of the slab rollback (Pownall et al.,
656 2013). Such a narrow rifted margin associated with lithospheric STEP fault defines a class of oblique margin that is
657 expected to be hardly preserved in the geological record due the transient nature of retreating subduction systems.

658

659

660 **Data availability.** This study is based on data compilation. Data used in this study can be found in the appropriate
661 references. Paleostress tensors obtained by the inversion of fault slip data are available online in the Supplement.

662

663 **Supplement.** The supplement related to this article is available on-line at:

664

665 **Competing interests.** The authors declare that they have no conflict of interest.

666 **Authors contribution**

667 ML and FM, conceptualize, prepared figures and tables, compiled and interpreted field structural data and wrote the
668 paper. DC provided and interpreted the seismic lines, reviewed the text and contributed to the writing. AJ carefully
669 examined the implementation of his numerical results and reviewed the text. EM, SC and VM, supervised and
670 coordinate the different project tasks and reviewed the text.

671 **Acknowledgments**

672 Víctor Tendero Salmerón, Guillermo Booth-Rea, and an anonymous reviewers are warmly thanked for their comments
673 that greatly improved the manuscript. Editors J. Phethean and S. Buiter are thanks for handling the manuscript. The
674 stereogram results were obtained using Win-Tensor, a software developed by Dr. Damien Delvaux, Royal Museum
675 for Central Africa, Tervuren, Belgium (Delvaux and Sperner, 2003). The processed seismic data were interpreted
676 using Kingdom IHS Suite© software. This research benefited from discussions and support of OROGEN project, an
677 academic-industry research consortium between TOTAL, CNRS and BRGM.

678

679

- 681 Angrand, P., Mouthereau, F., 2021. Evolution of the Alpine orogenic belts in the Western Mediterranean region as
682 resolved by the kinematics of the Europe-Africa diffuse plate boundary. *Bsgf - Earth Sci Bulletin*.
683 <https://doi.org/10.1051/bsgf/2021031>
- 684 Argus, D.F., Gordon, R.G., DeMets, C., 2011. Geologically current motion of 56 plates relative to the no-net-
685 rotation reference frame. *Geochemistry, Geophysics, Geosystems* 12. <https://doi.org/10.1029/2011gc003751>
- 686 Augier, R., 2004. Evolution tardi-orogénique des Cordillères Bétiques (Espagne) : apports d'une étude intégrée 1
687 vol., [II]-400 p.
- 688 Augier, R., Agard, P., Monié, P., Jolivet, L., Robin, C., Booth-Rea, G., 2005. Exhumation, doming and slab retreat in
689 the Betic Cordillera (SE Spain): in situ $^{40}\text{Ar}/^{39}\text{Ar}$ ages and P-T-t paths for the Nevado-Filabride complex.
690 *Journal of Metamorphic Geology* 23, 357–381. <https://doi.org/10.1111/j.1525-1314.2005.00581.x>
- 691 Augier, R., Booth-Rea, G., Agard, P., Martínez-Martínez, J.M., Jolivet, L., Azañón, J.M., 2005a. Exhumation
692 constraints for the lower Nevado-Filabride Complex (Betic Cordillera, SE Spain): a Raman thermometry and
693 Tweequ multiequilibrium thermobarometry approach. *Bulletin de la Societe Geologique de France* 176, 403–
694 416. <https://doi.org/10.2113/176.5.403>
- 695 Augier, R., Jolivet, L., Couto, D.D., Negro, F., 2013. From ductile to brittle, late- to post-orogenic evolution of the
696 Betic Cordillera: Structural insights from the northeastern Internal zones. *Bulletin De La Société Géologique De*
697 *France* 184, 405–425. <https://doi.org/10.2113/gssgfbull.184.4-5.405>
- 698 Augier, R., Jolivet, L., Robin, C., 2005b. Late Orogenic doming in the eastern Betic Cordilleras: Final exhumation
699 of the Nevado-Filabride complex and its relation to basin genesis. *Tectonics* 24, n/a-n/a.
700 <https://doi.org/10.1029/2004tc001687>
- 701 Badji, R., Charvis, P., Bracene, R., Galve, A., Badsı, M., Ribodetti, A., Benaissa, Z., Klingelhoefer, F., Medaouri,
702 M., Beslier, M.-O., 2014. Geophysical evidence for a transform margin offshore Western Algeria: a witness of a
703 subduction-transform edge propagator? *Geophys J Int* 200, 1029–1045. <https://doi.org/10.1093/gji/ggu454>
- 704 Barcos, L., Balanyá, J.C., Díaz-Azpiroz, M., Expósito, I., Jiménez-Bonilla, A., 2015. Kinematics of the Torcal Shear
705 Zone: Transpressional tectonics in a salient-recess transition at the northern Gibraltar Arc. *Tectonophysics* 663,
706 62–77. <https://doi.org/10.1016/j.tecto.2015.05.002>
- 707 Baudouy, L., Haughton, P.D.W., Walsh, J.J., 2021. Evolution of a Fault-Controlled, Deep-Water Sub-Basin,
708 Tabernas, SE Spain. *Frontiers Earth Sci* 9, 767286. <https://doi.org/10.3389/feart.2021.767286>.
- 709 Bessière, E., Jolivet, L., Augier, R., Scaillet, S., Précigout, J., Azañón, J.-M., Crespo-Blanc, A., Masini, E., Couto,
710 D.D., 2021. Lateral variations of pressure-temperature evolution in non-cylindrical orogens and 3-D subduction
711 dynamics: the Betic-Rif Cordillera example. *Bsgf - Earth Sci Bulletin*. <https://doi.org/10.1051/bsgf/2021007>
- 712 Bezada, M.J., Humphreys, E.D., Toomey, D.R., Harnafi, M., Dávila, J.M., Gallart, J., 2013. Evidence for slab
713 rollback in westernmost Mediterranean from improved upper mantle imaging. *Earth and Planetary Science*
714 *Letters* 368, 51–60. <https://doi.org/10.1016/j.epsl.2013.02.024>
- 715 Booth-Rea, G., Martínez-Martínez, J.M., Giacomia, F., 2015. Continental subduction, intracrustal shortening, and
716 coeval upper-crustal extension: P-T evolution of subducted south Iberian paleomargin metapelites (Betics, SE
717 Spain). *Tectonophysics* 663, 122–139. <https://doi.org/10.1016/j.tecto.2015.08.036>
- 718 Booth-Rea, G., Ranero, C.R., Grevemeyer, I., 2018. The Alboran volcanic-arc modulated the Messinian faunal
719 exchange and salinity crisis. *Scientific reports* 8, 13015. <https://doi.org/10.1038/s41598-018-31307-7>
- 720 Booth-Rea, G., Ranero, C.R., Martínez-Martínez, J.M., Grevemeyer, I., 2007. Crustal types and Tertiary tectonic
721 evolution of the Alborán sea, western Mediterranean. *Geochemistry, Geophysics, Geosystems* 8, n/a-n/a.
722 <https://doi.org/10.1029/2007gc001639>
- 723 Booth-Rea, G., Azañón, J.-M., Azor, A., García-Dueñas, V., 2004a. Influence of strike-slip fault segmentation on
724 drainage evolution and topography. A case study: the Palomares Fault Zone (southeastern Betics, Spain). *J*
725 *Struct Geol* 26, 1615–1632. <https://doi.org/10.1016/j.jsg.2004.01.007>
- 726 Booth-Rea, G., Azañón, J.M., García-Dueñas, V., 2004b. Extensional tectonics in the northeastern Betics (SE
727 Spain): case study of extension in a multilayered upper crust with contrasting rheologies. *Journal of structural*
728 *geology* 26, 2039–2058. <https://doi.org/10.1016/j.jsg.2004.04.005>
- 729 Borque, M.J., Alzola, A.S., Martín-Rojas, I., Alfaro, P., Molina, S., Cintas, S.R., Caderot, G.R., Lacy, C., Avilés,
730 M., Olmo, A.H., Tortosa, F.J.G., Estévez, A., Gil, A.J., 2019. How Much Nubia-Eurasia Convergence Is
731 Accommodated by the NE End of the Eastern Betic Shear Zone (SE Spain)? Constraints From GPS Velocities.
732 *Tectonics* 38, 271–1839. <https://doi.org/10.1029/2018tc004970>
- 733 Braga, J.C., Martín, J.M., Quesada, C., 2003. Patterns and average rates of late Neogene–Recent uplift of the Betic
734 Cordillera, SE Spain. *Geomorphology* 50, 3–26. [https://doi.org/10.1016/s0169-555x\(02\)00205-2](https://doi.org/10.1016/s0169-555x(02)00205-2)

735 Carbonell, R., Sallares, V., Pous, J., Dañoibeitia, J.J., Queralt, P., Ledo, J.J., Dueñas, V.G., 1998. A multidisciplinary
736 geophysical study in the Betic chain (southern Iberia Peninsula). *Tectonophysics* 288, 137–152.
737 [https://doi.org/10.1016/s0040-1951\(97\)00289-8](https://doi.org/10.1016/s0040-1951(97)00289-8)

738 Clark, S.J.P., Dempster, T.J., 2009. The record of tectonic denudation and erosion in an emerging orogen: an apatite
739 fission-track study of the Sierra Nevada, southern Spain. *Journal of the Geological Society* 166, 87–100.
740 <https://doi.org/10.1144/0016-76492008-041>

741 Comas, M. C., J. J. Dañoibeitia, J. Alvarez-Marón, and J. I. Soto (1995), Crustal reflections and structure in the
742 Alboran Basin. Preliminary results of the ESCI-Alboran survey, *Rev. Soc. Geol. Esp.*, 8(4), 529 – 542.

743 Comas, M.C., García-Dueñas, V., Jurado, M.J., 1992. Neogene tectonic evolution of the Alboran Sea from MCS
744 data. *Geo-mar Lett* 12, 157–164. <https://doi.org/10.1007/bf02084927>

745 Comas, M., and MARSIBAL 1-06 Scientific Party (2007). Preliminary results of Marsibal 1-06 cruise in the
746 Alboran and western Algero-Balearic basins. *Geophys. Res. Abst.*, 9, 10871.

747 Conand, C., Mouthereau, F., Ganne, J., Lin, A.T., Lahfid, A., Daudet, M., Mesalles, L., Giletycz, S., Bonzani, M.,
748 2020. Strain Partitioning and Exhumation in Oblique Taiwan Collision: Role of Rift Architecture and Plate
749 Kinematics. *Tectonics* 39, e2019TC005798. <https://doi.org/10.1029/2019tc005798>

750 Crespo-Blanc, A., Comas, M., Balanyá, J.C., 2016. Clues for a Tortonian reconstruction of the Gibraltar Arc:
751 Structural pattern, deformation diachronism and block rotations. *Tectonophysics* 683, 308–324.
752 <https://doi.org/10.1016/j.tecto.2016.05.045>

753 d’Acremont, E., Lafosse, M., Rabaute, A., Teurquety, G., Couto, D.D., Ercilla, G., Juan, C., Lépinay, B.M.,
754 Lafuerza, S., Galindo-Zaldívar, J., Estrada, F., Vazquez, J.T., Leroy, S., Poort, J., Ammar, A., Gorini, C., 2020.
755 Polyphase Tectonic Evolution of Fore-Arc Basin Related to STEP Fault as Revealed by Seismic Reflection Data
756 From the Alboran Sea (W-Mediterranean). *Tectonics* 39. <https://doi.org/10.1029/2019tc005885>

757 Dalziel, I.W.D., Lawver, L.A., Norton, I.O., Gahagan, L.M., 2013. The Scotia Arc: Genesis, Evolution, Global
758 Significance. *Annu Rev Earth Pl Sc* 41, 767–793. <https://doi.org/10.1146/annurev-earth-050212-124155>

759 Daudet, M., Mouthereau, F., Bricchau, S., Crespo-Blanc, A., Gautheron, C., Angrand, P., 2020. Tectono-
760 Stratigraphic and Thermal Evolution of the Western Betic Flysch: Implications for the Geodynamics of South
761 Iberian Margin and Alboran Domain. *Tectonics* 39. <https://doi.org/10.1029/2020tc006093>

762 Dewey, J.F., 1988. Extensional collapse of orogens. *Tectonics* 7, 1123–1139.
763 <https://doi.org/10.1029/tc007i006p01123>

764 Dewey, J.F., Helman, M.L., Knott, S.D., Turco, E., Hutton, D.H.W., 1989. Kinematics of the western
765 Mediterranean. Geological Society, London, Special Publications 45, 265–283.
766 <https://doi.org/10.1144/gsl.sp.1989.045.01.15>

767 Diaz, J., Gallart, J., Carbonell, R., 2016. Moho topography beneath the Iberian-Western Mediterranean region
768 mapped from controlled-source and natural seismicity surveys. *Tectonophysics* 692, 74–85.
769 <https://doi.org/10.1016/j.tecto.2016.08.023>

770 Do Couto, D., Gumiaux, C., Augier, R., Leuret, N., Folcher, N., Jouannic, G., Jolivet, L., Suc, J., Gorini, C., 2014.
771 Tectonic inversion of an asymmetric graben: Insights from a combined field and gravity survey in the Sorbas
772 basin. *Tectonics* 33, 1360–1385. <https://doi.org/10.1002/2013tc003458>

773 Duggen, S., Hoernle, K., Bogaard, P. van den, Rüpke, L., Morgan, J.P., 2003. Deep roots of the Messinian salinity
774 crisis. *Nature* 422, 602–606. <https://doi.org/10.1038/nature01553>

775 Duggen, S., Hoernle, K., Bogaard, P. van den, Harris, C., 2004. Magmatic evolution of the Alboran region: The role
776 of subduction in forming the western Mediterranean and causing the Messinian Salinity Crisis. *Earth Planet Sc*
777 *Lett* 218, 91–108. [https://doi.org/10.1016/s0012-821x\(03\)00632-0](https://doi.org/10.1016/s0012-821x(03)00632-0)

778 Duggen, S., Hoernle, K., Klügel, A., Geldmacher, J., Thirlwall, M., Hauff, F., Lowry, D., Oates, N., 2008.
779 Geochemical zonation of the Miocene Alborán Basin volcanism (westernmost Mediterranean): geodynamic
780 implications. *Contrib Mineral Petr* 156, 577. <https://doi.org/10.1007/s00410-008-0302-4>

781 Echeverría, A., Khazaradze, G., Asensio, E., Gárate, J., Dávila, J.M., Suriñach, E., 2013. Crustal deformation in
782 eastern Betics from CuaTeNeo GPS network. *Tectonophysics* 608, 600–612.
783 <https://doi.org/10.1016/j.tecto.2013.08.020>

784 Ercilla, G., Galindo-Zaldívar, J., Estrada, F., Valencia, J., Juan, C., Casas, D., Alonso, B., Comas, M.C., Tendero-
785 Salmerón, V., Casalbore, D., Azpiroz-Zabala, M., Bárcenas, P., Ceramicola, S., Chiocci, F.L., Idárraga-García,
786 J., López-González, N., Mata, P., Palomino, D., Rodríguez-García, J.A., Teixeira, M., Nespereira, J., Vázquez,
787 J.T., Yenes, M., 2022. Understanding the complex geomorphology of a deep sea area affected by continental
788 tectonic indentation: The case of the Gulf of Vera (Western Mediterranean). *Geomorphology* 402, 108126.
789 <https://doi.org/10.1016/j.geomorph.2022.108126>

790 Faccenna, C., Becker, T.W., Auer, L., Billi, A., Boschi, L., Brun, J.P., Capitanio, F.A., Funicello, F., Horvath, F.,
791 Jolivet, L., Piromallo, C., Royden, L., Rossetti, F., Serpelloni, E., 2014. Mantle dynamics in the Mediterranean.
792 *Rev Geophys* 52, 283–332. <https://doi.org/10.1002/2013rg000444>
793 Fortuin, A.R., Krijgsman, W., 2003. The Messinian of the Nijar Basin (SE Spain): sedimentation, depositional
794 environments and paleogeographic evolution. *Sediment Geol* 160, 213–242. [https://doi.org/10.1016/s0037-](https://doi.org/10.1016/s0037-0738(02)00377-9)
795 [0738\(02\)00377-9](https://doi.org/10.1016/s0037-0738(02)00377-9)
796 Fossen, H., Teyssier, C., Whitney, D.L., 2013. Transtensional folding. *Journal of structural geology* 56, 89–102.
797 <https://doi.org/http://dx.doi.org/10.1016/j.jsg.2013.09.004>
798 Fossen, H., Tikoff, B., 1998. Extended models of transpression and transtension, and application to tectonic settings.
799 Geological Society, London, Special Publications 135, 15–33. <https://doi.org/10.1144/gsl.sp.1998.135.01.02>
800 Galindo-Zaldivar, J., Gonzalez-Lodeiro, F., Jabaloy, A., 2015. Progressive extensional shear structures in a
801 detachment contact in the Western Sierra Nevada (Betic Cordilleras, Spain). *Geodin Acta* 3, 73–85.
802 <https://doi.org/10.1080/09853111.1989.11105175>
803 Galindo-Zaldivar, J., Gil, A.J., Borque, M.J., González-Lodeiro, F., Jabaloy, A., Marin-Lechado, C., Ruano, P.,
804 Galdeano, C.S. de, 2003. Active faulting in the internal zones of the central Betic Cordilleras (SE, Spain). *J*
805 *Geodyn* 36, 239–250. [https://doi.org/10.1016/s0264-3707\(03\)00049-8](https://doi.org/10.1016/s0264-3707(03)00049-8)
806 Gallais, F., Graindorge, D., Gutscher, M.-A., Klaeschen, D., 2013. Propagation of a lithospheric tear fault (STEP)
807 through the western boundary of the Calabrian accretionary wedge offshore eastern Sicily (Southern Italy).
808 *Tectonophysics* 602, 141–152. <https://doi.org/10.1016/j.tecto.2012.12.026>
809 Garcia-Castellanos, D., Villaseñor, A., 2012. Messinian salinity crisis regulated by competing tectonics and erosion
810 at the Gibraltar arc. *Nature* 480, 359–363. <https://doi.org/10.1038/nature10651>
811 García-Dueñas, V., Banda, E., Torné, M., Córdoba, D., Group, E.-B.W., 1994. A deep seismic reflection survey
812 across the Betic Chain (southern Spain): first results. *Tectonophysics* 232, 77–89. [https://doi.org/10.1016/0040-](https://doi.org/10.1016/0040-1951(94)90077-9)
813 [1951\(94\)90077-9](https://doi.org/10.1016/0040-1951(94)90077-9)
814 Giaconia, F., Booth-Rea, G., Martínez-Martínez, J.M., Azañón, J.M., Pérez-Peña, J.V., Pérez-Romero, J., Villegas,
815 I., 2012. Geomorphic evidence of active tectonics in the Sierra Alhamilla (eastern Betics, SE Spain).
816 *Geomorphology* 145, 90–106. <https://doi.org/10.1016/j.geomorph.2011.12.043>
817 Giaconia, F., Booth-Rea, G., Martínez-Martínez, J.M., Azañón, J.M., Pérez-Romero, J., Villegas, I., 2013. Mountain
818 front migration and drainage captures related to fault segment linkage and growth: The Polopos transpressive
819 fault zone (southeastern Betics, SE Spain). *J Struct Geol* 46, 76–91. <https://doi.org/10.1016/j.jsg.2012.10.005>
820 Giaconia, F., Booth-Rea, G., Martínez-Martínez, J.M., Azañón, J.M., Storti, F., Artoni, A., 2014. Heterogeneous
821 extension and the role of transfer faults in the development of the southeastern Betic basins (SE Spain).
822 *Tectonics* 33, 2467–2489. <https://doi.org/10.1002/2014tc003681>
823 Giaconia, F., Booth-Rea, G., Ranero, C.R., Gràcia, E., Bartolome, R., Calahorrano, A., Iacono, C.L., Vendrell,
824 M.G., Cameselle, A.L., Costa, S., Peña, L.G. de la, Martínez-Lorient, S., Perea, H., Viñas, M., 2015.
825 Compressional tectonic inversion of the Algero-Balearic basin: Latest Miocene to present oblique
826 convergence at the Palomares margin (Western Mediterranean): Tectonic Inversion of Palomares Margin.
827 *Tectonics* 34, 1516–1543. <https://doi.org/10.1002/2015tc003861>
828 Gomez-Pugnaire, M.T., Fernandez-Soler, J.M., 1987. High-pressure metamorphism in metabasites from the Betic
829 Cordilleras (S.E. Spain) and its evolution during the Alpine orogeny. *Contrib Mineral Petr* 95, 231–244.
830 <https://doi.org/10.1007/bf00381273>
831 Gómez de la Peña, L.G. de la, Grevemeyer, I., Kopp, H., Díaz, J., Gallart, J., Booth-Rea, G., Gràcia, E., Ranero,
832 C.R., 2020a. The Lithospheric Structure of the Gibraltar Arc System From Wide-Angle Seismic Data. *J Geophys*
833 *Res Solid Earth* 125. <https://doi.org/10.1029/2020jb019854>
834 Gómez de la Peña, L.G. de la, Ranero, C.R., Gràcia, E., 2018. The Crustal Domains of the Alboran Basin (Western
835 Mediterranean). *Tectonics* 37, 3352–3377. <https://doi.org/10.1029/2017tc004946>
836 Gómez de la Peña, L.G. de la, Ranero, C.R., Gràcia, E., Booth-Rea, G., 2020b. The evolution of the westernmost
837 Mediterranean basins. *Earth-sci Rev* 103445. <https://doi.org/10.1016/j.earscirev.2020.103445>
838 Govers, R., Wortel, M.J.R., 2005. Lithosphere tearing at STEP faults: response to edges of subduction zones. *Earth*
839 *Planet Sc Lett* 236, 505–523. <https://doi.org/10.1016/j.epsl.2005.03.022>
840 Haq, B., Gorini, C., Baur, J., Moneron, J., & Rubino, J.-L. (2020). Deep Mediterranean's Messinian evaporite giant:
841 How much salt? *Global and Planetary Change*, 184, 103052.
842 doi:<https://doi.org/10.1016/j.gloplacha.2019.103052>
843 Houghton, P.D.W., 2000. Evolving turbidite systems on a deforming basin floor, Tabernas, SE Spain.
844 *Sedimentology* 47, 497–518. <https://doi.org/10.1046/j.1365-3091.2000.00293.x>

845 Haughton, P.D.W., 1994. Deposits of deflected and ponded turbidity currents, Sorbas Basin, Southeast Spain. *J*
846 *Sediment Res* 64, 233–246. <https://doi.org/10.1306/d4267d6b-2b26-11d7-8648000102c1865d>

847 Heit, B., Mancilla, F. de L., Yuan, X., Morales, J., Stich, D., Martín, R., Molina-Aguilera, A., 2017. Tearing of the
848 mantle lithosphere along the intermediate-depth seismicity zone beneath the Gibraltar Arc: The onset of
849 lithospheric delamination. *Geophys Res Lett* 44, 4027–4035. <https://doi.org/10.1002/2017gl073358>

850 Hodgson, D.M., Haughton, P.D.W., 2004. Impact of syndepositional faulting on gravity current behaviour and deep-
851 water stratigraphy: Tabernas-Sorbas Basin, SE Spain. *Geological Soc Lond Special Publ* 222, 135–158.
852 <https://doi.org/10.1144/gsl.sp.2004.222.01.08>

853 Jabaloy-Sánchez, A., Talavera, C., Rodríguez-Peces, M.J., Vázquez-Vílchez, M., Evans, N.J., 2021. U-Pb
854 geochronology of detrital and igneous zircon grains from the Águilas Arc in the Internal Betics (SE Spain):
855 Implications for Carboniferous-Permian paleogeography of Pangea. *Gondwana Res* 90, 135–158.
856 <https://doi.org/10.1016/j.gr.2020.10.013>

857 Janowski, M., Loget, N., Gautheron, C., Barbarand, J., Bellahsen, N., Driessche, J.V. den, Babault, J., Meyer, B.,
858 2017. Neogene exhumation and relief evolution in the eastern Betics (SE Spain): Insights from the Sierra de
859 Gador. *Terra Nova* 29, 91–97. <https://doi.org/10.1111/ter.12252>

860 Johnson, C., Harbury, N., Hurford, A.J., 1997. The role of extension in the Miocene denudation of the Nevado-
861 Filábride Complex, Betic Cordillera (SE Spain). *Tectonics* 16, 189–204. <https://doi.org/10.1029/96tc03289>

862 Jolivet, L., Baudin, T., Calassou, S., Chevrot, S., Ford, M., Issautier, B., Lasseur, E., Masini, E., Manatschal, G.,
863 Mouthereau, F., Thionon, I., Vidal, O., 2021a. Geodynamic evolution of a wide plate boundary in the Western
864 Mediterranean, near-field versus far-field interactions. *Bsgf - Earth Sci Bulletin* 192, 48.
865 <https://doi.org/10.1051/bsgf/2021043>

866 Jolivet, L., Faccenna, C., 2000. Mediterranean extension and the Africa-Eurasia collision. *Tectonics* 19, 1095–1106.
867 <https://doi.org/10.1029/2000tc900018>

868 Jolivet, L., Menant, A., Roche, V., Le Pourhiet, L., Maillard, A., Augier, R., Couto, D.D., Gorini, C., Thionon, I.,
869 Canva, A., 2021b. Transfer zones in Mediterranean back-arc regions and tear faults. *Bsgf - Earth Sci Bulletin*
870 192, 11. <https://doi.org/10.1051/bsgf/2021006>

871 Jourdon, A., Kergaravat, C., Duclaux, G., Huguen, C., 2021. Looking beyond kinematics: 3D thermo-mechanical
872 modelling reveals the dynamics of transform margins. *Solid Earth* 12, 1211–1232. <https://doi.org/10.5194/se-12-1211-2021>

873

874 Juan, C., Ercilla, G., Javier Hernández-Molina, F., Estrada, F., Alonso, B., Casas, D., . . . Ammar, A. (2016).
875 Seismic evidence of current-controlled sedimentation in the Alboran Sea during the Pliocene and Quaternary:
876 Palaeoceanographic implications. *Marine Geology*, 378, 292-311.
877 doi:<https://doi.org/10.1016/j.margeo.2016.01.006>

878 Jurado, M.J., Comas, M.C., 1992. Well log interpretation and seismic character of the cenozoic sequence in the
879 northern Alboran Sea. *Geo-Marine Letters* 12, 129–136.

880 Kleverlaan, K., 1989. Neogene history of the Tabernas basin (SE Spain) and its Tortonian submarine fan
881 development. *Geologie en Mijnbouw* 421–432.

882 Kleverlaan, K., 1989. Three distinctive feeder-lobe systems within one time slice of the Tortonian Tabernas fan, SE
883 Spain. *Sedimentology* 36, 25–45. <https://doi.org/10.1111/j.1365-3091.1989.tb00818.x>

884 Kleverlaan, K., 1987. Gordo megabed: a possible seismite in a tortonian submarine fan, tabernas basin, province
885 almeria, southeast spain. *Sediment Geol* 51, 165–180. [https://doi.org/10.1016/0037-0738\(87\)90047-9](https://doi.org/10.1016/0037-0738(87)90047-9)

886 Koulali, A., Ouazar, D., Tahayt, A., King, R.W., Vernant, P., Reilinger, R.E., McClusky, S., Mourabit, T., Davila,
887 J.M., Amraoui, N., 2011. New GPS constraints on active deformation along the Africa–Iberia plate boundary.
888 *Earth Planet Sc Lett* 308, 211–217. <https://doi.org/10.1016/j.epsl.2011.05.048>

889 Larouzière, F.D.D., Bolze, J., Bordet, P., Hernandez, J., Montenat, C., d’Estevou, P.O., 1988. The Betic segment of
890 the lithospheric Trans-Alboran shear zone during the Late Miocene. *Tectonophysics* 152, 41–52.
891 [https://doi.org/10.1016/0040-1951\(88\)90028-5](https://doi.org/10.1016/0040-1951(88)90028-5)

892 Le Pourhiet, L., Huet, B., May, D.A., Labrousse, L., Jolivet, L., 2012. Kinematic interpretation of the 3D shapes of
893 metamorphic core complexes: 3D SHAPES OF MCCs. *Geochem Geophys Geosystems* 13.
894 <https://doi.org/10.1029/2012gc004271>.

895 Lonergan, L., White, N., 1997. Origin of the Betic-Rif mountain belt. *Tectonics* 16, 504–522.
896 <https://doi.org/10.1029/96tc03937>

897 Mancilla, F. de L., Booth-Rea, G., Stich, D., Pérez-Peña, J.V., Morales, J., Azañón, J.M., Martín, R., Giaconia, F.,
898 2015a. Slab rupture and delamination under the Betics and Rif constrained from receiver functions.
899 *Tectonophysics*. <https://doi.org/10.1016/j.tecto.2015.06.028>

900 Mancilla, F. de L., Heit, B., Morales, J., Yuan, X., Stich, D., Molina-Aguilera, A., Azañón, J.M., Martín, R., 2018.
901 A STEP fault in Central Betics, associated with lateral lithospheric tearing at the northern edge of the Gibraltar
902 arc subduction system. *Earth Planet Sc Lett* 486, 32–40. <https://doi.org/10.1016/j.epsl.2018.01.008>
903 Mancilla, F. de L., Stich, D., Morales, J., Martín, R., Diaz, J., Pazos, A., Córdoba, D., Pulgar, J.A., Ibarra, P.,
904 Harnafi, M., Gonzalez-Lodeiro, F., 2015b. Crustal thickness and images of the lithospheric discontinuities in the
905 Gibraltar arc and surrounding areas. *Geophysical Journal International* 203, 1804–1820.
906 <https://doi.org/10.1093/gji/ggv390>
907 Martín, J.M., Braga, J.C., Rivas, P., 1989. Coral successions in Upper Tortonian reefs in SE Spain. *Lethaia* 22, 271–
908 286. <https://doi.org/10.1111/j.1502-3931.1989.tb01342.x>
909 Martín, J.M., Braga, J.C., 1994. Messinian events in the Sorbas Basin in southeastern Spain and their implications in
910 the recent history of the Mediterranean. *Sediment Geol* 90, 257–268. [https://doi.org/10.1016/0037-](https://doi.org/10.1016/0037-0738(94)90042-6)
911 [0738\(94\)90042-6](https://doi.org/10.1016/0037-0738(94)90042-6)
912 Martínez-García, P., Comas, M., Lonergan, L., Watts, A.B., 2017. From Extension to Shortening: Tectonic
913 Inversion Distributed in Time and Space in the Alboran Sea, Western Mediterranean. *Tectonics* 36, 2777–2805.
914 <https://doi.org/10.1002/2017tc004489>
915 Martínez-García, P., Soto, J.I., Comas, M., 2011. Recent structures in the Alboran Ridge and Yusuf fault zones
916 based on swath bathymetry and sub-bottom profiling: evidence of active tectonics. *Geo-mar Lett* 31, 19–36.
917 <https://doi.org/10.1007/s00367-010-0212-0>
918 Martínez-Martínez, J.M., Azañón, J.M., 1997. Mode of extensional tectonics in the southeastern Betics (SE Spain):
919 Implications for the tectonic evolution of the peri-Alborán orogenic system. *Tectonics* 16, 205–225.
920 <https://doi.org/10.1029/97tc00157>
921 Martínez-Martínez, J.M., Booth-Rea, G., Azañón, J.M., Torcal, F., 2006. Active transfer fault zone linking a
922 segmented extensional system (Betics, southern Spain): Insight into heterogeneous extension driven by edge
923 delamination. *Tectonophysics* 422, 159–173. <https://doi.org/10.1016/j.tecto.2006.06.001>
924 Martínez-Martínez, J.M., Soto, J.I., Balanyá, J.C., 2002. Orthogonal folding of extensional detachments: Structure
925 and origin of the Sierra Nevada elongated dome (Betics, SE Spain). *Tectonics* 21, 3-1-3–20.
926 <https://doi.org/10.1029/2001tc001283>
927 Martínez-Martínez, J.M., Soto, J.I., Balanyá, J.C., 2004. Elongated domes in extended orogens: A mode of mountain
928 uplift in the Betics (southeast Spain), in: *Special Paper 380: Gneiss Domes in Orogeny*. Geological Society of
929 America, pp. 243–265. <https://doi.org/10.1130/0-8137-2380-9.243>
930 Martínez-Martos, M., Galindo-Zaldívar, J., Martínez-Moreno, F.J., Calvo-Rayó, R., Galdeano, C.S. de, 2017.
931 Superposition of tectonic structures leading elongated intramontane basin: the Alhabia basin (Internal Zones,
932 Betic Cordillera). *Int J Earth Sci* 106, 2461–2471. <https://doi.org/10.1007/s00531-016-1442-9>
933 Meighan, H.E., Brink, U. ten, Pulliam, J., 2013. Slab tears and intermediate-depth seismicity: slab tears and
934 intermediate seismicity. *Geophys Res Lett* 40, 4244–4248. <https://doi.org/10.1002/grl.50830>
935 Meijninger, B.M.L., Vissers, R.L.M., 2006. Miocene extensional basin development in the Betic Cordillera, SE
936 Spain revealed through analysis of the Alhama de Murcia and Crevillente Faults: Miocene extensional basin
937 development in the Betic Cordillera. *Basin Res* 18, 547–571. <https://doi.org/10.1111/j.1365-2117.2006.00308.x>
938 Montecat, C., D’Estevou, P.O., 1992. Geodynamics of the Eastern Betic late Neogene Basins. A Review. *Física de*
939 *la Tierra* 57–75.
940 Montecat, C., d’Estevou, P.O., 1999. The diversity of late Neogene sedimentary basins generated by wrench faulting
941 in the eastern Betic Cordillera, SE Spain. *J Petrol Geol* 22, 61–80. [https://doi.org/10.1111/j.1747-](https://doi.org/10.1111/j.1747-5457.1999.tb00459.x)
942 [5457.1999.tb00459.x](https://doi.org/10.1111/j.1747-5457.1999.tb00459.x)
943 Mora, M., 1993. Tectonic and sedimentary analysis of the Huerca-Overa region, South East Spain, Betic Cordillera.
944 University of Oxford, 300 pp.
945 Moragues, L., Ruano, P., Azañón, J.M., Garrido, C.J., Hidas, K., Booth-Rea, G., 2021. Two Cenozoic Extensional
946 Phases in Mallorca and Their Bearing on the Geodynamic Evolution of the Western Mediterranean. *Tectonics*
947 40. <https://doi.org/10.1029/2021tc006868>.
948 Mouthereau, F., Angrand, P., Jourdon, A., Ternois, S., Fillon, C., Calassou, S., Chevrot, S., Ford, M., Jolivet, L.,
949 Manatschal, G., Masini, E., Thion, I., Vidal, O., Baudin, T., 2021. Cenozoic mountain building and topographic
950 evolution in Western Europe: impact of billions of years of lithosphere evolution and plate kinematics. *Bsgf -*
951 *Earth Sci Bulletin* 192, 56. <https://doi.org/10.1051/bsgf/2021040>
952 Mouthereau, F., Filleaudeau, P., Vacherat, A., Pik, R., Lacombe, O., Fellin, M.G., Castelltort, S., Christophoul, F.,
953 Masini, E., 2014. Placing limits to shortening evolution in the Pyrenees: Role of margin architecture and
954 implications for the Iberia/Europe convergence. *Tectonics* 33, 2283–2314. <https://doi.org/10.1002/2014tc003663>

- 955 Neuharth, D., Brune, S., Glerum, A., Morley, C.K., Yuan, X., Braun, J., 2021. Flexural strike-slip basins. *Geology*.
956 <https://doi.org/10.1130/g49351.1>
- 957 Nocquet, J.-M., 2012. Present-day kinematics of the Mediterranean: A comprehensive overview of GPS results.
958 *Tectonophysics* 579, 220–242. <https://doi.org/10.1016/j.tecto.2012.03.037>
- 959 Okay, A.I., Tüysüz, O., Kaya, Ş., 2004. From transpression to transtension: changes in morphology and structure
960 around a bend on the North Anatolian Fault in the Marmara region. *Tectonophysics* 391, 259–282.
961 <https://doi.org/10.1016/j.tecto.2004.07.016>
- 962 Palano, M., González, P.J., Fernández, J., 2015. The Diffuse Plate boundary of Nubia and Iberia in the Western
963 Mediterranean: Crustal deformation evidence for viscous coupling and fragmented lithosphere. *Earth and
964 Planetary Science Letters* 430, 439–447. <https://doi.org/10.1016/j.epsl.2015.08.040>
- 965 Palano, M., González, P.J., Fernández, J., 2013. Strain and stress fields along the Gibraltar Orogenic Arc:
966 Constraints on active geodynamics. *Gondwana Res* 23, 1071–1088. <https://doi.org/10.1016/j.gr.2012.05.021>
- 967 Palomeras, I., Thurner, S., Levander, A., Liu, K., Villaseñor, A., Carbonell, R., Harnafi, M., 2014. Finite-frequency
968 Rayleigh wave tomography of the western Mediterranean: Mapping its lithospheric structure. *Geochemistry,
969 Geophysics, Geosystems* 15, 140–160. <https://doi.org/10.1002/2013gc004861>
- 970 Pedrera, A., Galindo-Zaldívar, J., Galdeano, C.S. de, López-Garrido, Á.C., 2007. Fold and fault interactions during
971 the development of an elongated narrow basin: The Almanzora Neogene-Quaternary Corridor (SE Betic
972 Cordillera, Spain): FOLD AND FAULT INTERACTIONS. *Tectonics* 26, n/a-n/a.
973 <https://doi.org/10.1029/2007tc002138>
- 974 Pedrera, A., Galindo-Zaldívar, J., Ruiz-Constán, A., Duque, C., Marín-Lechado, C., Serrano, I., 2009. Recent large
975 fold nucleation in the upper crust: Insight from gravity, magnetic, magnetotelluric and seismicity data (Sierra de
976 Los Filabres–Sierra de Las Estancias, Internal Zones, Betic Cordillera). *Tectonophysics* 463, 145–160.
977 <https://doi.org/10.1016/j.tecto.2008.09.037>
- 978 Pedrera, A., Galindo-Zaldívar, J., Tello, A., Marín-Lechado, C., 2010. Intramontane basin development related to
979 contractional and extensional structure interaction at the termination of a major sinistral fault: The Huércal-
980 Overa Basin (Eastern Betic Cordillera). *J Geodyn* 49, 271–286. <https://doi.org/10.1016/j.jog.2010.01.008>
- 981 Pickering, K.T., Hodgson, D.M., Platzman, E., Clark, J.D., Stephens, C., 2001. A New Type of Bedform Produced
982 by Backfilling Processes in a Submarine Channel, Late Miocene, Tabernas-Sorbas Basin, SE Spain. *J Sediment
983 Res* 71, 692–704. <https://doi.org/10.1306/2dc40960-0e47-11d7-8643000102c1865d>
- 984 Pindell, J.L., Kennan, L., 2009. Tectonic evolution of the Gulf of Mexico, Caribbean and northern South America in
985 the mantle reference frame: an update. *Geological Soc Lond Special Publ* 328, 1–55.
986 <https://doi.org/10.1144/sp328.1>
- 987 Platt, J.P., Behr, W.M., Johannesen, K., Williams, J.R., 2013. The Betic-Rif Arc and Its Orogenic Hinterland: A
988 Review. *Annual Review of Earth and Planetary Sciences* 41, 313–357. <https://doi.org/10.1146/annurev-earth-050212-123951>
- 989 Platt, J.P., Kelley, S.P., Carter, A., Orozco, M., 2005. Timing of tectonic events in the Alpujarride Complex, Betic
990 Cordillera, southern Spain. *J Geol Soc London* 162, 451–462. <https://doi.org/10.1144/0016-764903-039>
- 991 Platt, J.P., Whitehouse, M.J., Kelley, S.P., Carter, A., Hollick, L., 2003. Simultaneous extensional exhumation
992 across the Alboran Basin: Implications for the causes of late orogenic extension. *Geology* 31, 251–254.
993 [https://doi.org/10.1130/0091-7613\(2003\)031<0251:seeata>2.0.co;2](https://doi.org/10.1130/0091-7613(2003)031<0251:seeata>2.0.co;2)
- 994 Platt, J.P., Anczkiewicz, R., Soto, J.-I., Kelley, S.P., Thirlwall, M., 2006. Early Miocene continental subduction and
995 rapid exhumation in the western Mediterranean. *Geology* 34, 981–984. <https://doi.org/10.1130/g22801a.1>
- 996 Platt, J.P., Vissers, R.L.M., 1989. Extensional collapse of thickened continental lithosphere: A working hypothesis
997 for the Alboran Sea and Gibraltar arc. *Geology* 17, 540–543. [https://doi.org/10.1130/0091-7613\(1989\)017<0540:ecotcl>2.3.co;2](https://doi.org/10.1130/0091-7613(1989)017<0540:ecotcl>2.3.co;2)
- 998 Platt, J.P., Whitehouse, M.J., 1999. Early Miocene high-temperature metamorphism and rapid exhumation in the
999 Betic Cordillera (Spain): evidence from U–Pb zircon ages. *Earth and Planetary Science Letters* 171, 591–605.
- 1000 Platzman, E.S., 1992. Paleomagnetic rotations and the kinematics of the Gibraltar arc. *Geology* 20, 311–314.
1001 [https://doi.org/10.1130/0091-7613\(1992\)020<0311:pratko>2.3.co;2](https://doi.org/10.1130/0091-7613(1992)020<0311:pratko>2.3.co;2)
- 1002 Poisson, A., Guezou, J.C., Ozturk, A., Inan, S., Temiz, H., Gürsöy, H., Kavak, K.S., ÖZDEN, S., 1996. Tectonic
1003 Setting and Evolution of the Sivas Basin, Central Anatolia, Turkey. *International Geology Review* 38, 838–853.
1004 <https://doi.org/10.1080/00206819709465366>
- 1005 Poisson, A.M., Morel, J.L., Andrieux, J., Coulon, M., Wernli, R., Guernet, C., 1999. The origin and development of
1006 neogene basins in the SE Betic Cordillera (SE Spain): a case study of the Tabernas-Sorbas and Huercal Overa
1007 basins. *J Petrol Geol* 22, 97–114. <https://doi.org/10.1111/j.1747-5457.1999.tb00461.x>
- 1008
1009

1010 Pownall, J.M., Hall, R., Watkinson, I.M., 2013. Extreme extension across Seram and Ambon, eastern Indonesia:
1011 evidence for Banda slab rollback. *Solid Earth* 4, 277–314. <https://doi.org/10.5194/se-4-277-2013>

1012 Rat, J., Mouthereau, F., Brichau, S., Crémedes, A., Bernet, M., Balvay, M., Ganne, J., Lahfid, A., Gautheron, C.,
1013 2019. Tectonothermal Evolution of the Cameros Basin: Implications for Tectonics of North Iberia. *Tectonics* 38,
1014 440–469. <https://doi.org/10.1029/2018tc005294>

1015 Rat, J., Mouthereau, F., Brichau, S., Vacherat, A., Fillon, C., Gautheron, C., 2022. Timing and distribution of
1016 exhumation in the Ebro basin reveal a plate-scale 10 Ma geodynamic event. *Global Planet Change* 103973.
1017 <https://doi.org/10.1016/j.gloplacha.2022.103973>

1018 Reicherter, K., Hübscher, C., 2006. Evidence for a seafloor rupture of the Carboneras Fault Zone (southern Spain):
1019 Relation to the 1522 Almería earthquake? *J Seismol* 11, 15–26. <https://doi.org/10.1007/s10950-006-9024-0>

1020 Reinhardt, L.J., Dempster, T.J., Shroder, J.F., Persano, C., 2007. Tectonic denudation and topographic development
1021 in the Spanish Sierra Nevada. *Tectonics* 26, n/a-n/a. <https://doi.org/10.1029/2006tc001954>

1022 Richards, J.P., 2009. Postsubduction porphyry Cu-Au and epithermal Au deposits: Products of remelting of
1023 subduction-modified lithosphere. *Geology* 37, 247–250. <https://doi.org/10.1130/g25451a.1>

1024 Riding, R., Braga, J.C., Martín, J.M., Sánchez-Almazo, I.M., 1998. Mediterranean Messinian Salinity Crisis:
1025 constraints from a coeval marginal basin, Sorbas, southeastern Spain. *Mar Geol* 146, 1–20.
1026 [https://doi.org/10.1016/s0025-3227\(97\)00136-9](https://doi.org/10.1016/s0025-3227(97)00136-9)

1027 Rodríguez-Fernández, J., Azor, A., Azañón, J.M., 2012. Tectonics of Sedimentary Basins 461–479.
1028 <https://doi.org/10.1002/9781444347166.ch23>

1029 Romagny, A., Jolivet, L., Menant, A., Bessièrre, E., Maillard, A., Canva, A., Gorini, C., Augier, R., 2020. Detailed
1030 tectonic reconstructions of the Western Mediterranean region for the last 35 Ma, insights on driving
1031 mechanisms. *Bsgf - Earth Sci Bulletin* 191, 37. <https://doi.org/10.1051/bsgf/2020040>

1032 Rosenbaum, G., Lister, G.S., Duboz, C., 2002. Relative motions of Africa, Iberia and Europe during Alpine
1033 orogeny. *Tectonophysics* 359, 117–129. [https://doi.org/10.1016/s0040-1951\(02\)00442-0](https://doi.org/10.1016/s0040-1951(02)00442-0)

1034 Sanz de Galdeano, C.S., Vera, J.A., 1992. Stratigraphic record and palaeogeographical context of the Neogene
1035 basins in the Betic Cordillera, Spain. *Basin Res* 4, 21–36. <https://doi.org/10.1111/j.1365-2117.1992.tb00040.x>

1036 Sanz de Galdeano, C.S.D., Rodríguez-Fernández, J., López-Garrido, A.C., 1985. A strike-slip fault corridor within
1037 the Alpujarra Mountains (Betic Cordilleras, Spain). *Geol Rundsch* 74, 641–655.
1038 <https://doi.org/10.1007/bf01821218>

1039 Sanz de Galdeano, C.S. de, Alfaro, P., 2004. Tectonic significance of the present relief of the Betic Cordillera.
1040 *Geomorphology* 63, 175–190. <https://doi.org/10.1016/j.geomorph.2004.04.002>

1041 Scotney, P., Burgess, R., Rutter, E.H., 2000. 40Ar/39Ar age of the Cabo de Gata volcanic series and displacements
1042 on the Carboneras fault zone, SE Spain. *J Geol Soc London* 157, 1003–1008.
1043 <https://doi.org/10.1144/jgs.157.5.1003>

1044 Sosson, M., Morrillon, A.-C., Bourgeois, J., Féraud, G., Poupeau, G., Saint-Marc, P., 1998. Late exhumation stages
1045 of the Alpujarride Complex (western Betic Cordilleras, Spain): new thermochronological and structural data on
1046 Los Reales and Ojen nappes. *Tectonophysics* 285, 253–273. [https://doi.org/10.1016/s0040-1951\(97\)00274-6](https://doi.org/10.1016/s0040-1951(97)00274-6)

1047 Spakman, W., Wortel, R., 2004. The TRANSMED Atlas. The Mediterranean Region from Crust to Mantle 31–52.
1048 https://doi.org/10.1007/978-3-642-18919-7_2

1049 Spakman, W., Chertova, M.V., Berg, A. van Hinsbergen, D.J.J., 2018. Puzzling features of western Mediterranean
1050 tectonics explained by slab dragging. *Nat Geosci* 11. <https://doi.org/10.1038/s41561-018-0066-z>

1051 Stich, D., Serpelloni, E., Mancilla, F. de L., Morales, J., 2006. Kinematics of the Iberia–Maghreb plate contact from
1052 seismic moment tensors and GPS observations. *Tectonophysics* 426, 295–317.
1053 <https://doi.org/10.1016/j.tecto.2006.08.004>

1054 Tendero-Salmerón, V., Galindo-Zaldívar, J., d’Acremont, E., Catalán, M., Martos, Y.M., Ammar, A., Ercilla, G.,
1055 2022. New insights on the Alboran Sea basin extension and continental collision from magnetic anomalies
1056 related to magmatism (western Mediterranean). *Mar Geol* 443, 106696.
1057 <https://doi.org/10.1016/j.margeo.2021.106696>

1058 Teyssier, C., Tikoff, B., 1998. Strike-slip partitioned transpression of the San Andreas fault system: a lithospheric-
1059 scale approach. *Geological Soc Lond Special Publ* 135, 143–158. <https://doi.org/10.1144/gsl.sp.1998.135.01.10>

1060 Vacherat, A., Mouthereau, F., Pik, R., Bellahsen, N., Gautheron, C., Bernet, M., Daudet, M., Balansa, J., Tibari, B.,
1061 Jamme, R.P., Radal, J., 2016. Rift-to-collision transition recorded by tectonothermal evolution of the northern
1062 Pyrenees. *Tectonics* 35, 907–933. <https://doi.org/10.1002/2015tc004016>

1063 van Hinsbergen, D.J.J., Vissers, R.L.M., Spakman, W., 2014. Origin and consequences of western Mediterranean
1064 subduction, rollback, and slab segmentation. *Tectonics* 33, 393–419. <https://doi.org/10.1002/2013tc003349>

1065 Vázquez, M., Jabaloy, A., Barbero, L., Stuart, F.M., 2011. Deciphering tectonic- and erosion-driven exhumation of
1066 the Nevado-Filábride Complex (Betic Cordillera, Southern Spain) by low temperature thermochronology:
1067 Deciphering tectonic- and erosion-driven exhumation. *Terra Nova* 23, 257–263. [https://doi.org/10.1111/j.1365-](https://doi.org/10.1111/j.1365-3121.2011.01007.x)
1068 [3121.2011.01007.x](https://doi.org/10.1111/j.1365-3121.2011.01007.x)

1069 Vergés, J., Fernández, M., 2012. Tethys–Atlantic interaction along the Iberia–Africa plate boundary: The Betic–Rif
1070 orogenic system. *Tectonophysics* 579, 144–172. <https://doi.org/10.1016/j.tecto.2012.08.032>

1071 Vernant, P., Fadil, A., Mourabit, T., Ouazar, D., Koulali, A., Davila, J.M., Garate, J., McClusky, S., Reilinger, R.,
1072 2010. Geodetic constraints on active tectonics of the Western Mediterranean: Implications for the kinematics and
1073 dynamics of the Nubia-Eurasia plate boundary zone. *J Geodyn* 49, 123–129.
1074 <https://doi.org/10.1016/j.jog.2009.10.007>

1075 Villasenor, A., Chevrot, S., Harnafi, M., Gallart, J., Pazos, A., Serrano, I., Córdoba, D., Pulgar, J.A., Ibarra, P.,
1076 2015. Subduction and volcanism in the Iberia–North Africa collision zone from tomographic images of the
1077 upper mantle. *Tectonophysics*. <https://doi.org/10.1016/j.tecto.2015.08.042>

1078 Waldner, M., Bellahsen, N., Mouthereau, F., Bernet, M., Pik, R., Rosenberg, C.L., Balvay, M., 2021. Central
1079 Pyrenees Mountain Building: Constraints From New LT Thermochronological Data From the Axial Zone.
1080 *Tectonics* 40. <https://doi.org/10.1029/2020tc006614>

1081 Weijermars, R., Roep, Th.B., Eeckhout, B.V. den, Postma, G., Kleverlaan, K., 1985. Uplift history of a Betic fold
1082 nappe inferred from Neogene-Quaternary sedimentation and tectonics (in the Sierra Alhamilla and Almería,
1083 Sorbas and Tabernas Basins of the Betic Cordilleras, SE Spain). *Geologie en Mijnbouw* 397–411.

1084 Zeck, H.P., Monié, P., Villa, I.M., Hansen, B.T., 1992. Very high rates of cooling and uplift in the Alpine belt of the
1085 Betic Cordilleras, southern Spain. *Geology* 20, 79. [https://doi.org/10.1130/0091-](https://doi.org/10.1130/0091-7613(1992)020<0079:vhroca>2.3.co;2)
1086 [7613\(1992\)020<0079:vhroca>2.3.co;2](https://doi.org/10.1130/0091-7613(1992)020<0079:vhroca>2.3.co;2)

1087